Mediterranean coastal wave-climate long-term trend in climate change scenarios and effects on the optimal sizing of OWC wave

Mediterranean coastal wave-climate long-term trend in climate change scenarios and effects on the optimal sizing of OWC wave energy converters / Irene Simonetti, Lorenzo Cappietti. - In: COASTAL ENGINEERING. - ISSN 0378-3839. - ELETTRONICO. - 179:(2023), pp. 104247.0-104247.17. [10.1016/j.coastaleng.2022.104247]

Published version:
DOI: 10.1016/j.coastaleng.2022.104247

(Article begins on next page)

Coastal Engineering 179 (2023) 104247

Contents lists available at ScienceDirect

Coastal Engineering

journal homepage: www.elsevier.com/locate/coastaleng

Mediterranean coastal wave-climate long-term trend in climate change scenarios and effects on the optimal sizing of OWC wave energy converters

Irene Simonetti *, Lorenzo Cappietti

Department of Civil and Environmental Engineering, Università degli Studi di Firenze, 50139, Firenze, Italy

A R T I C L E I N F O

Keywords:
Long-term trends
Climate change effects
Oscillating water column
Geometry optimization
Wave energy conversion
Ocean wave response to climate change

A B S T R A C T

This work assesses the effect of long-term changes in the wave climate on the optimal sizing and performances of oscillating water column wave energy converters along the coastline of the Mediterranean basin. Trends are evaluated based on the projections of future wave climate to 2100 delivered by the Climate Data Store of the Copernicus Climate Change Service under representative atmospheric emission scenarios. The capture width of the device under different wave conditions is computed using an empirical model capable of predicting the device performance with acceptable accuracy and limited computational time. The optimal geometry of the device varies significantly across different geographical locations, with maximum values of chamber size along the north African coasts and western Sardinia and Corse, and minimum values in the Adriatic and Aegean Seas. Long-term changes in the wave energy resource result in moderate modifications of the optimal geometry, with relative variations between present and future scenarios up to 10% of the size. The annual energy production of the device in the projected scenario would significantly increase in most geographical locations, potentially contributing to reducing the levelized cost of energy and favouring the economic competitiveness of this technology.

1. Introduction

The topic of hindcasting and projection of the wave climate is fundamental for design studies of offshore and coastal structures and it is currently an open field of research, as proved, e.g., in some recent works (Morim et al., 2019; O'Grady et al., 2021; Salvadori et al., 2020). Ocean waves show a complex response to climate change, which may have a direct influence on the variables connected to their generation, transformation, and dissipation (e.g., wind patterns). The Intergovernmental Panel for Climate Change (IPCC) identified ocean waves, in combination with other marine processes potentially affected by long-term climate dynamics (e.g. sea-level rise), as one of the key climate drivers of coastal hazards (IPCC, 2013; IPCC, 2019). The Fifth Assessment Report (AR5) of the IPCC (IPCC, 2013) formulated projections of climate scenarios induced by different paths in the future Greenhouses Gasses (GHC) emissions, defined as Representative Concentration Pathways (RCPs). RCP4.5 and RCP8.5 represent, respectively: (i) a scenario with a projected radiative forcing of 4.5 Wm^{-2}, comprising the stabilization of GHG emissions before 2100 and (ii) a scenario with 8.5 Wm^{-2} of radiative forcing, foreseeing a continuous increase of GHG emissions throughout the century.

Several studies analysed regional or global scale projections of the wave climate, aiming to identify long-term effects of climate change on ocean waves, focusing either on mean annual values, high quantiles and annual maxima of significant wave heights and periods or on extreme wave conditions. The robustness and reliability of the projected change in the wave climate are still under debate (Morim et al., 2019). Generally, a greater degree of consensus exists about the projected change in mean annual values, while the trend of extreme events has a higher uncertainty (Lobeto et al., 2021).

Morim et al. (2018) analysed the results of available regional or global-scale wave climate projections (from 91 different sources), aiming to assess the related uncertainties. The authors pointed out a general agreement on an increasing trend for annual mean values of significant wave height in the eastern Pacific, the Southern Ocean and Baltic Sea and on an opposite decreasing trend for the North Atlantic and the Mediterranean Sea. Concerning extreme wave height values, a generalized lack of consensus was found, except for consistent projections of increase for the Southern Ocean and decrease for the north Atlantic area.

More recently, De Leo et al., 2021a analysed the projected wave

* Corresponding author.
E-mail address: irene.simonetti@unifi.it (I. Simonetti).

https://doi.org/10.1016/j.coastaleng.2022.104247
Received 2 May 2022; Received in revised form 4 October 2022; Accepted 30 October 2022
Available online 3 November 2022

climate change under the RPC8.5 scenario in the Mediterranean Sea. The authors used the wave model WavewatchIII forced by an ensemble of seven different Euro-CORDEX climate projections. Results showed a decreasing trend of annual means and annual maxima of significant wave height and mean periods over most of the Mediterranean basin. Lobeto et al. (2021) also analysed a seven-member ensemble of wave climate simulations, documenting relevant divergences between the detected trends for mean and extreme wave conditions in several ocean regions. Focusing on the Mediterranean area, the authors highlighted a moderate (<1 m) increase in the projected 20-years return period wave height for the western Mediterranean basin and an opposite decrease in the eastern Mediterranean Sea. In contrast, annual mean values of significant wave height were found to decrease over most of the basin. At present, most of the available studies focus on significant wave height, while long term trends in wave period and direction are less investigated.

In this wide framework, concerns about GHG emissions related to climate change are among the principal drivers of the increasing attention toward renewable energy sources. Wave energy conversion could potentially accelerate the process of energy transition towards zero-carbon, contributing to a climate-neutral energy supply. At present, different technical and non-technical issues limit the development of wave energy conversion (Farrell et al., 2015; Ramos and Ringwood, 2016), de-facto confining it to the pre-commercial stage. Among such issues, a noteworthy factor is the need to reduce the Levelised Cost of Energy (LCOE) which is a function of Capital and Operating Expenditures (CAPEX and OPEX) and of the average Annual Energy Production (AEP) of the device over its lifetime (Garcia-Teruel and Forehand, 2021). Assessing investments in the wave energy conversion sector based on LCOE is a well-established practice (de Andres et al., 2017). Reliable estimations of the AEP achievable with a certain Wave Energy Converter (WEC) are, therefore, essential for a sound evaluation of LCOE in the investment decision-making process. In turn, the lack of reliability in estimates of the device productivity is also a result of the uncertainty in the assessment of the available wave energy resource (Mackay et al., 2010; Robertson et al., 2019), since the geometry of the device which maximizes the AEP is fundamentally dependent on wave climate in the foreseen installation site (de Andres et al., 2016).

Uncertainties on the wave resource may be related to different aspects, e.g. (i) the number of years of available data for the assessment, (ii) whether such data are produced by a numerical model or from field measurements, (iii) the physical processes represented by the numerical model used, (iv) the resolution in time, space and frequency and the parametrization of the spectral wave information (Robertson et al., 2019; Mérigaud and Ringwood, 2018; de Andrés et al., 2015). The aforementioned projections of climate-change related long-term trends in the wave climate add to the overall resource uncertainty.

On the other hand, a reliable evaluation of AEP also requires modelling the considered WEC, using numerical or theoretical approaches capable of accounting for all the relevant physical phenomena influencing the WEC functioning, including real fluid effects and nonlinear dynamics (Penalba et al., 2017). Aiming to assess the WEC performance under different wave conditions (which is required to properly estimate the AEP), computationally efficient models of the device are needed. This need becomes particularly pressing for performing optimization studies.

Available studies on the optimization of the geometry of WECs are based on hindcast wave data, i.e. they only consider past wave climate. A previous attempt to evaluate the impact of wave trends on the optimization of a WEC was presented in Ulazia et al. (2020), with regard to the North-East Atlantic Ocean areas of Europe and Africa. The optimal width of the considered WEC, i.e. an Oscillating Water Column (OWC) (Falcão and Henriques, 2016), was shown to vary considerably in different installation locations and over time. However, assessing data between 1979 and 2018, this study did not consider the projected change in the wave conditions included in the IPCC's climate change scenarios.

The present work focuses on evaluating the effects induced by wave climate long-term changes, as projected in the RPC8.5 IPCC scenario, on optimal geometry and power production of OWC-WEC devices that could be located along the Mediterranean Sea coastline. The empirical model proposed by Simonetti et al., 2018a, is used to evaluate the OWC performance (in terms of efficiency of the primary conversion process) under different wave conditions. The empirical model, based on regression analysis on an extensive database of laboratory tests and numerical simulations, explicitly provides the performance of rectangular shaped, asymmetric and bottom-detached OWC devices given the wave conditions, the water depth, the geometrical parameters of the device and the turbine damping as input variables. The model can effectively be used for this kind of study since it allows to implicitly account for non-linear phenomena, which may relevantly influence the device's functioning, while maintaining a low computational cost. Explicitly considering the effect of projected changes in the wave climate on the optimal sizing and performance of OWC-WEC, the paper addresses a specific gap of knowledge in the present literature.

The remainder of the paper is structured as follows: material and methods are introduced at first, regarding the wave data used to assess the present and future wave climates, the methodology adopted to evaluate eventual trends in wave data and the procedure used to optimize the OWC geometry for a given wave climate. Results are then presented and discussed, in terms of trends detected in the wave energy resource, optimal size and energy production of OWCs in the present wave climate and the effect of long-term trends on said parameters. Finally, concluding remarks are given.

2. Materials and methods

2.1. Wave data

Time series of hourly wave data for the European coastline along the 20 m bathymetric contour, with a horizontal resolution of ~30 km, are provided by the Climate Data Store (CDS) (Caires and Yan, 2022) of the Copernicus Climate Change Service (C3S). Wave data available in the CDS are obtained using the *European Center of Medium-range Weather Forecast* (ECMWF) wave forecasting system, which is based on the spectral wave model WAM (Komen et al., 1994). The ECMWF version of WAM (Gunther et al., 1992), referred to as SAW, uses the source term parametrization for wave growth and dissipation denoted ST4 (Ardhuin et al., 2010). The validation of SAW wave hindcast data against observations is documented in (ECMWF, 2019). Being specifically conceived as a tool to assess the impact of climate change on the ocean waves, SAW data include three climate scenarios: a historical reanalysis based on ERA5 data (covering the period 1976–2017), and two Representative Concentration Pathway (RCP) scenarios, covering the period 2040–2100, as defined by the IPPC, i.e. RCP4.5 and RCP8.5. The wave climate in these scenarios is simulated using wind forcing from the Euro-CORDEX climate model ensemble (the HIRHAM5 regional climate model). ERA5 is the fifth generation atmospheric reanalysis of the global climate provided by ECMWF (Hersbach et al., 2020) and it is judged to provide one of the most accurate atmospheric forcings for modelling wind waves (Sharmar et al., 2021).

CDS-C3S database provides the spectral peak period T_p, while the spectral period $T_{m-1,0}$, which denotes the period of a single sinusoidal wave that contains the same amount of energy as the reference sea state, is not provided. Therefore $T_{m-1,0}$ is determined from the available peak period T_p assuming a theoretical shape of the wave energy spectrum, allowing to obtain $T_{m-1,0} = \alpha\, T_p$. Assuming a JONSWAP spectrum with a peak enhancement factor $\gamma = 3.3$, a value of $\alpha = 0.904$ is obtained. This constant α-value is used the present work.

2.2. Trend analysis

For each grid point on the 20 m bathymetric contour along the whole Mediterranean coast, wave data are analysed to assess the presence of significant trends in the following parameters: annual maximum values of H_{m0} and $T_{m-1,0}$ (H_{m0}^{max} and $T_{m-1,0}^{max}$), annual mean values of H_{m0} and $T_{m-1,0}$ (H_{m0}^{mean} and $T_{m-1,0}^{mean}$), annual values of the 90th percentile of H_{m0} and $T_{m-1,0}$ (H_{m0}^{90th} and $T_{m-1,0}^{90th}$). In addition, trends in the values of wave period and height associated with the greatest fraction of the wave energy (H_{m0}^{maxAE} and $T_{m-1,0}^{maxAE}$) on an annual basis, are also considered, given the relevance of these parameters on the optimization of the performance of WECs. To obtain these values, the annual wave data are preliminarily analysed in the form of a Scatter Matrix (SM), representing the bivariate distributions of occurrences of sea states defined by pairs of H_{m0} and $T_{m-1,0}$ and their corresponding Annual Energy (AE). For each pair of H_{m0} and $T_{m-1,0}$, the associated wave power per meter of wavefront P_{wave} [W/m] is computed, and the AE is obtained based on the relative frequency of occurence of the pair. The values of H_{m0} and $T_{m-1,0}$ having the highest contribution, as a percentage, to the total annual incident energy are then selected as H_{m0}^{maxAE} and $T_{m-1,0}^{maxAE}$. To jointly account for eventual variations in significant wave height and periods, trends in the annual mean values of available wave power P_{wave} are also examined. P_{wave} is computed as in Eq. (1).

$$P_{wave} = \frac{1}{16}\rho \cdot g \cdot H_{m0}^{2} \cdot C_g \tag{1}$$

where ρ is the water density, g is gravitational acceleration, Cg is the wave group velocity obtained by solving the linear dispersion relation on the considered water depth h. The wave energy period $T_{m-1,0}$ is assumed as reference period to compute the value of Cg. It is worth mentioning that Eq. (1) provides an approximation of the exact wave power of irregular waves of a given spectrum on a finite water depth. The errors induced by adopting such approximation on wave power assessments were proved to be negligible (i.e., lower than 5%) compared to the exact computation (Sheng and Li, 2017). Moreover, being the spectral parameters unknown in CDS-C3S dataset, the use of Eq. (1) is justified.

The presence of a trend in the wave climate, and the entity and significance of the trend, are assessed on the 1976–2100 time series (with a gap between 2017 and 2041, where Copernicus CDS-C3S data are not available) of the aforementioned parameters by using the following statistical indicators, widely used in hydrology and meteorology fields (Helsel et al., 2020):

(i) Theil-Sen's slope s (Sen, 1968), a robust nonparametric estimator of the trend in sample data, computed as the median of all possible slopes among couples of points, as in Eq. (2);

$$s = median\left(\frac{y_j - y_i}{x_j - x_i}\right) \quad \forall\, i < j,\ i = 1, 2, ..., (n-1),\ j = 2, 3, ..., n \tag{2}$$

where y_j, y_i denotes the j-th and i-th data in the time series, and x_j and x_i are the corresponding reference times.

(ii) p-value of Mann-Kendall tests (Kendall, 1938), allowing to assess to what extent data are consistent with the null hypothesis (i.e. the absence of long-term trends): for p-values close to 1, data are consistent with the null hypothesis, while p-values close to 0 denote the presence of a significant trend affecting the data.

Theil-Sen's slope s values indicate where trends of a certain magnitude will most probably happen, while the significance of trends can be evaluated based on Mann-Kandall's p-value. The combined use of these two statistical indicators to detect trends in wave data has already been proved to be a reliable methodological approach (De Leo et al., 2021a; De Leo et al., 2021b).

2.3. OWC-WEC and multi-regression-model of the performance

The present study considers fixed, bottom-detached and asymmetric OWC devices. The OWC is a well-established concept for wave energy conversion (as reviewed in Falcão and Henriques, 2016), with some full-scale prototype installation in Europe, e.g. the pilot plant on the island of Pico, Azores (Falcão et al., 2020), the Mutriko plant, Spain (Ibarra-Berastegi et al., 2021), the REWEC3 in Civitavecchia (Arena et al., 2017).

In its fixed version, the OWC system consists of a hydraulic structure, i.e. a partially submerged caisson, connected to a Power Take Off (PTO) system, generally an air turbine and an electrical generator. The wave-induced motion of the water inside the caisson expands and compresses the air in the upper part of the caisson. The pneumatic power of the generated airflow (primary conversion process) drives the PTO system (secondary and tertiary conversions) (Fig. 1).

The hydrodynamic performance of the OWC device is traditionally expressed in terms of capture width ratio (CW*), defined as the ratio of the wave energy extracted by the OWC device, P_{owc}, to the incident wave energy, P_{wave}, as in Eq. (3).

$$CW^* = \frac{P_{owc}}{P_{wave} \cdot B} \tag{3}$$

where B is the width of the device perpendicular to wave propagation direction. In the present study, P_{owc} refers to the fraction of wave energy converted into pneumatic energy, i.e., only the efficiency of the primary conversion process is considered.

CW^* is intensely affected by the wave climate, underling the importance of a site-specific design, as discussed e.g. in Simonetti et al. (2017), and Ciappi et al. (2022). These previous studies underlined that: (i) the value of damping applied on the hydraulic caisson by the PTO which maximizes CW^* strongly depends on the chamber length W and the relative water depth kh (being k the wavenumber and h the water depth); (ii); the draft of front wall D influences both the OWC resonance frequency and the wave-induced pressure acting on it; (iii) an optimal value of the OWC chamber length in wave direction relative to the incident wavelength, W/λ, exists; (iv) when determining the optimal sizing and performance of OWCs, a strong mutual interaction takes place between the aforementioned parameters, implying the need for a combined optimization of geometry and PTO damping.

In the present study, values of CW^* under the action of incident waves are computed by using the empirical Multi-Regression Model (MRM) proposed by Simonetti et al. (2018a). The model explicitly

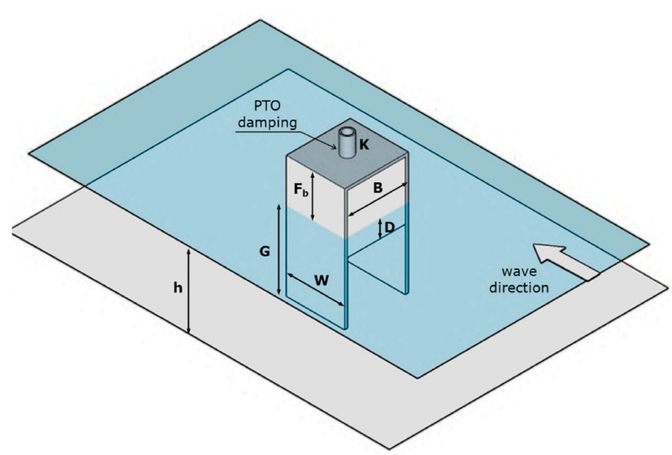

Fig. 1. Definition sketch of the design parameters for a fixed, bottom-detached and asymmetric OWC wave energy converter.

provides values of CW^* of a rectangular shaped, fixed, bottom-detached and asymmetric OWC device given the wave conditions (H_{m0} and $T_{m-1,0}$), the water depth h, the geometrical parameters of the OWC (W, D and B) and the PTO damping (K) as input variables. By using pi-theorem and dimensional analysis, CW^* is expressed as a function of the following dimensionless parameters (generically denoted by *)

$$CW^* = f(h^*, W^*, D^*, K^*) \tag{4}$$

where the function f is provided by the MRM. Dimensionless parameters are defined as follows:

$$h^* = kh \tag{5}$$

$$D^* = D \bigg/ \left(H \cdot \frac{\cosh k(h-D)}{\cosh(kh)} \right) \tag{6}$$

$$W^* = W/_{\lambda} \tag{7}$$

$$K^* = K \cdot B \cdot W / \rho_a^{1/2} \tag{8}$$

where the wave number k is univocally related to the wavelength λ and period T, on a given h, by the linear dispersion relation. The model was formulated based on regression analysis, and it implicitly includes non-linear effects observed in the numerical and experimental datasets used to derive it. It has to be stressed that the application of the MRM should be limited to the range of dimensionless parameters used for its formulation (i.e.: h^*=1.5–3.5, D^*=1.8–5, W^*=0.08–0.2, K^*=20–170). The MRM was formulated with reference to an OWC chamber having the following side ratios: $0.67<B/W<2$. Moreover, the ratio of the sub-merged length of the OWC back wall to the incident wavelength varied between $0.11 < G/\lambda < 0.30$, corresponding to ratios of the gap between the sea-bottom and the OWC back wall to the wavelength of $0.08<(h-G)/\lambda < 0.21$. The readers are referred to Simonetti et al., 2018a, for further details on the model formulation, validation and applicability limits. The functions f describing the MRM are also reported in *Appendix I* for the sake of clarity. Recently, the MRM has been successfully used by Ulazia et al. (2020), and Gubesch et al. (2022), confirming its functionality in preliminary optimization processes of OWC devices.

2.4. Methodology for selecting the optimal OWC geometry

In each of the available points on the 20 m bathymetric contour along the whole Mediterranean Sea coastline, the MRM is used to obtain the CW^* of the device over a range of H_{m0} and $T_{m-1,0}$ pairs, each pair representing a cell of the scatter matrix SM. SMs are obtained, in each geographical location, based on 30 years of hourly wave data, considering two alternative scenarios for a comparative evaluation: a present scenario, comprising data from 1986 to 2016, and a future scenario, obtained with data from 2071 to 2100. For the future wave climate, the projections under RCP8.5 emission scenarios are considered, as it represents conditions in which the greatest changes are expected compared to the current scenario. For the MRM application, SMs are discretized in bins of 0.125 m and 0.125 s, for H_{m0} and $T_{m-1,0}$, respectively. A direct search approach is used, defining the parameter space to explore as the set of all possible combinations of W, D and K-values, within a prefixed range. Values of W between 7 and 11.5 m, D between 3.5 and 6 m (with a discretization step of 0.2 m) and K between 0.6 and 1.5 $kg^{1/2}m^{-7/2}$ (with a discretization step of 0.04 $kg^{1/2}m^{-7/2}$) are considered. The following parameters of the OWC are kept constant: chamber width perpendicular to wave direction B=10 m, freeboard Fb=8 m, length of the lateral al back walls G=14.5 m (i.e., the OWC is detached from the bottom of 5.5 m). The range of OWC parameters, as well as H_{m0}, $T_{m-1,0}$ pairs ($1<H_{m0}<5.5$ m and $4.4<T_{m-1,0}<9.2$ s, respectively), have been selected to respect the range of applicability of the MRM (Simonetti et al., 2018a). Since the empirical MRM is developed based on data relative to regular waves only, the assumption of approximating the wave climate in each considered site by means of a set of regular waves with height $H=H_{m0}/\sqrt{2}$ and period $T=T_{m-1,0}$ is made, ensuring the equivalence of the energy flux related to regular waves and irregular waves.

In each of the geographical locations considered, the geometry (identified as a combination of W, D, K) associated with the highest AEP is selected as optimal. The AEP of the device is defined as the weighted average of the device capture width ratio CW^*_n obtained for each of the n pairs of H_{m0} and $T_{m-1,0}$ considered from the reference SM, with weights being the annual energy of each of the n pairs, AE_n (Eq. (9)). $(AEP)_i$ is the annual energy extracted in the form of pneumatic energy by the OWC device having geometry defined by the set of parameters $(W, D, K)_i$.

$$(AEP)_i = \left(\frac{\sum_n CW_n^* \cdot AE_n}{\sum_n AE_n} \right)_i \tag{9}$$

To account for the decrease in the OWC performance caused by possible air intake at the front draft during the passage of wave trough (inlet broaching phenomena), a reduction factor equal to 0.5 is applied to the value of CW^* predicted by the MRM for $H_{m0}>D$. It is worth to point out that further specific studies should be carried out to precisely quantified the value of the reduction factor of CW^* due to inlet broaching phenomena, here only tentatively assumed as constantly equal to 0.5. Since the main aim of the present work is to provide a comparative assessment of the OWC performance under different wave climate scenarios, the impact of such an assumption on the results is considered relatively limited.

In an effort to provide indications about the geographical locations more suitable for the installation of OWC devices with features similar to those considered in this study, the LCOE of each geometry alternative is also examined. Assuming a lifetime of the device m of 25 years, the LCOE is computed based on Eq. 10

$$LCOE = \left(CAPEX + \sum_{t=1}^{m} \frac{OPEX_t}{(1+j)^t} \right) \bigg/ \sum_{t=1}^{m} \frac{AEP_t}{(1+j)^t} \tag{10}$$

where the weighted average cost of capital j is assumed equal to 10% (Chozas, 2015), CAPEX is assumed given by: (i) a component proportional to the volume of material needed to build the device, (ii) a fixed component for the cost of the PTO system (Falcão, 2004). OPEX is supposed to account for 4% of CAPEX (assumed as a reference value in the literature range of 1.5–9% (Têtu, Fernandez Chozas, 2021). An accurate economic analysis, fundamental for a quantitative assessment of the LCOE, is out of the scope of the present research. Therefore, aiming to provide only comparative indications about the more suitable locations, values of LCOE normalized between 0 and 1 will be presented in this work.

3. Results

Results of the trend analysis performed on CDS-C3S wave data on the 20 m contour of the Mediterranean Sea are presented at first, considering all the available data in the period 1976–2100. Then, the optimal sizing of the OWC device and the related pneumatic AEP are obtained for each grid point in the present scenario (i.e., based on the SM obtained for the 30-years data from 1986 to 2016). Finally, possible modifications of the OWC functioning deriving from using SMs based on projections of future wave climate for the 30-years period 2071–2100 are analysed in *Section 3.3*.

3.1. Trends in the available wave resource

Concerning the mean annual significant wave height, H_{m0}^{mean}, positive values of Theil-Sen's slope s (denoting upward trends) are observed especially for the Alboran Sea close to the Strait of Gibraltar, in front of Spain and Morocco, and in the Aegean Sea (Fig. 2, a). In these areas, the

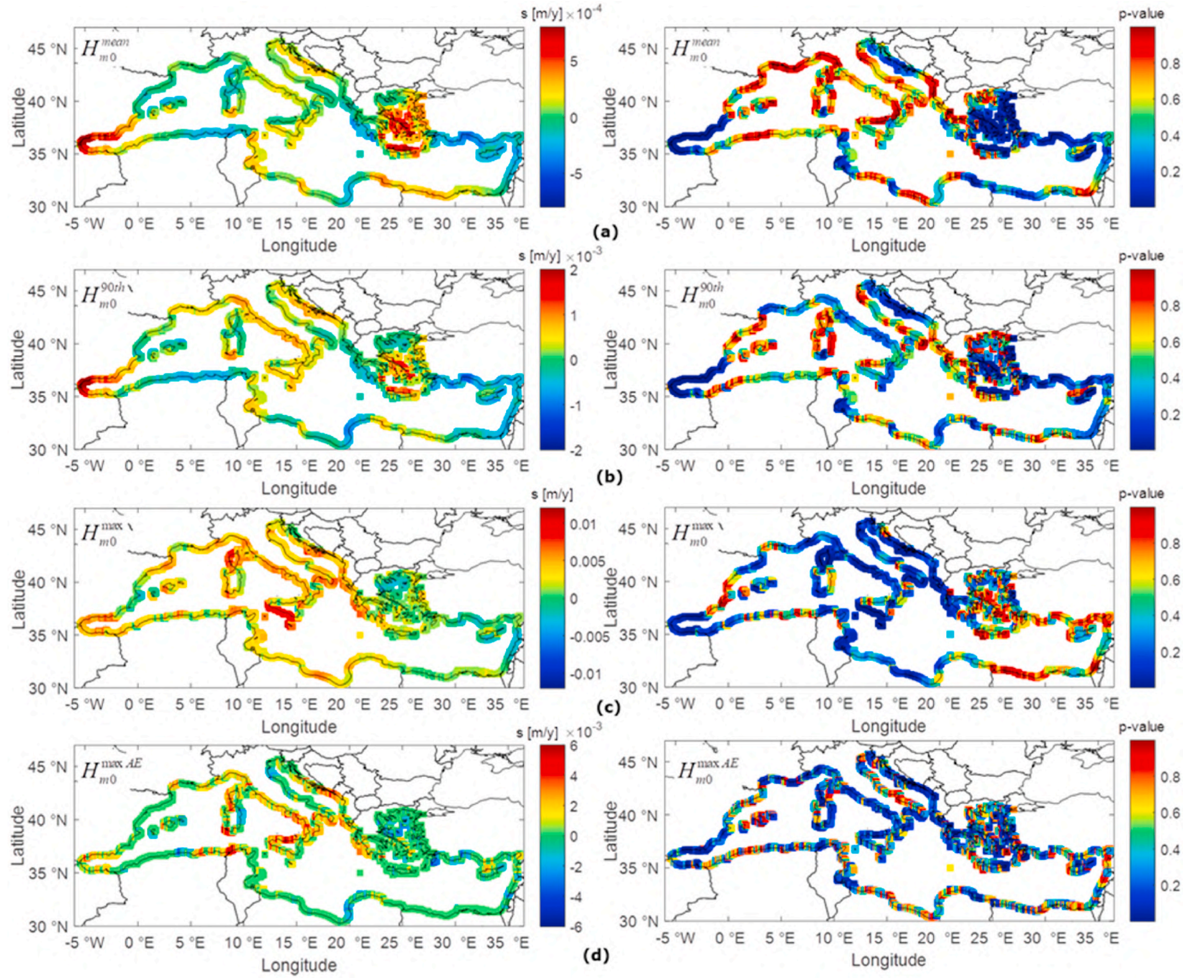

Fig. 2. Spatial distribution of Theil-Sen's slope *s* (left) and *p*-value of Mann-Kandall tests (rigth) in the IPCC's RCP8.5 scenario for: annual mean significant wave height H_{m0}^{mean} (a), 90th percentile of significant wave height H_{m0}^{90th} (b), annual maximum H_{m0}^{max} (c), wave height with the highest contribution to the total annual energy H_{m0}^{maxAE} (d).

magnitude of the trend is limited, i.e. up to $9 \cdot 10^{-4}$ m/year. In the same locations, moderate positive trends for annual means of H_{m0} were also highlighted in De Leo et al. (2021a). Although limited in magnitude, the positive trends in H_{m0}^{mean} can be considered significant, being associated with *p*-values close to zero (Fig. 2,a, right). Absent or slightly decreasing trends in H_{m0}^{mean} are found in the Northern Mediterranean coast of Spain and France, in that of Algeria and in the Eastern Levantine Sea, as well as along most of the Italian coasts. In these areas, the absence of significant trends on H_{m0}^{mean} is confirmed by *p*-values closer to 1. A significant, albeit limited in magnitude (*s* up to $-4 \cdot 10^{-4}$ m/year), decreasing trend is found along the southern Turkish coasts and around Cyprus.

Annual values of the 90th percentile wave height H_{m0}^{90th} (Fig. 2,b) show a higher magnitude of the positive trend in the Alboran Sea close to the Strait of Gibraltar and in the Aegean Sea (where Theil-Sen's slope *s* attains values of $2 \cdot 10^{-3}$ m/year). Based on *p*-values, these trends can be considered significant. A moderate ($s < 1 \cdot 10^{-3}$ m/year) positive trend in H_{m0}^{90th} is observed also for most of the coasts in front of France and in the Tyrrhenian Sea. A decreasing trend in H_{m0}^{90th} is found, instead, in wide homogeneous areas in the north Africa (especially Algeria) and the eastern Levantine Sea.

Focusing on annual maximum wave heights, H_{m0}^{max}, the western coasts of Corse and Sicily show the highest positive trends, with s-values up to $10 \cdot 10^{-3}$ m/year and high significance levels based on *p*-values (Fig. 2,c). In the Strait of Gibraltar, a positive trend with a lower magnitude (up to $6 \cdot 10^{-3}$ m/year) is found for H_{m0}^{max}. Trends are scarcely significant in most of the remaining areas. In general, trends of annual maxima are more geographically dispersed compared to lower percentiles or mean values of H_{m0} (as previously pointed out also in the work of De Leo et al. (2021a), especially along the north African coasts of Algeria and Tunisia. Concerning the wave height associated to the greatest fraction of the wave energy (H_{m0}^{maxAE}), a null trend is noticed in the vast majority of locations on the 20 m contours (Fig. 2,d). Positive trends are scattered over isolated points, without geographically extended homogenous trends.

Similar spatial distributions for annual average values of the energy period, $T_{m-1,0}^{mean}$, are observed close to the Strait of Gibraltar, with significant (*p*-values∼0) upwards trends characterized by *s*-values $\sim 2 \cdot 10^{-3}$ s/year (Fig. 3,a). Negative and significant trends on $T_{m-1,0}^{mean}$ are observed on the western coasts of Corse and Sardinia, on the north of Sicily and in the eastern Ionian Sea close to Greece and Albania. In the same geographical areas, negative trends are not observed, instead, when considering the higher percentile of $T_{m-1,0}$ ($T_{m-1,0}^{90th}$) or annual maxima ($T_{m-1,0}^{max}$) (Fig. 3,b-c). Indeed, for annual maxima $T_{m-1,0}^{max}$, Theil-Sen's slope *s* attains the higher positive values, reaching up to 10^{-2} s/year in the Ligurian, Libyan and Levantine seas, with high significance level over quite extended homogenous geographical areas confirmed by *p*-values close to 0. In the Alboran Sea close to the Strait of Gibraltar (Fig. 3,c), $T_{m-1,0}^{max}$ has an opposite (i.e. decreasing) trend compared to that observed for $T_{m-1,0}^{mean}$ and $T_{m-1,0}^{90th}$ in the same zone. However, *p*-values in

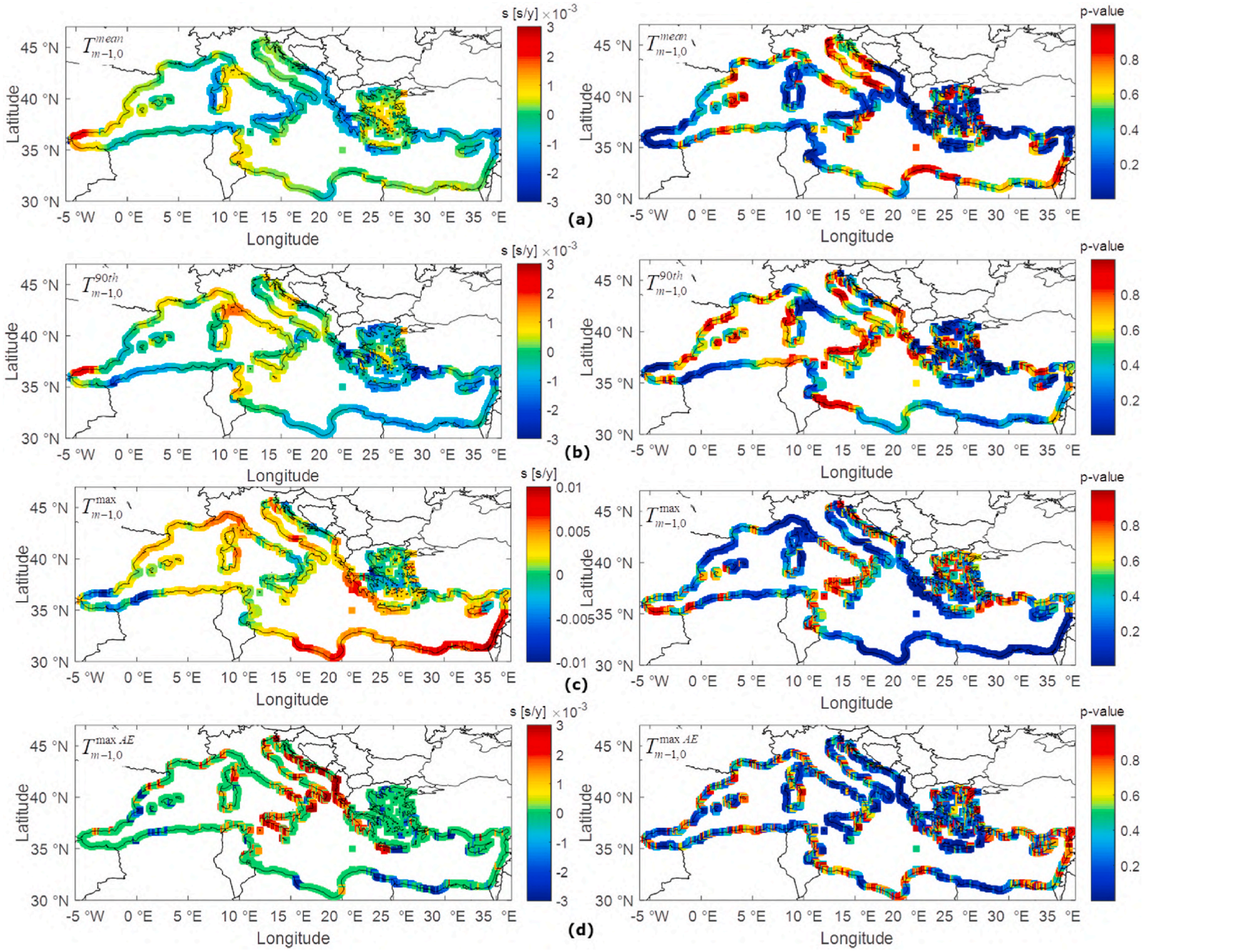

Fig. 3. Spatial distribution of Theil-Sen's slope *s* (left) and *p*-value of Mann-Kandall tests (right) in the IPCC's RCP8.5 scenario for: annual mean energy period $T_{m-1,0}^{mean}$ (a), 90th percentile of energy period $T_{m-1,0}^{90th}$ (b), annual maximum value of energy period $T_{m-1,0}^{max}$ (c), energy period with the highest contribution to the total annual energy $T_{m-1,0}^{maxAE}$ (d).

these locations suggest that the negative trend of annual maximum periods is scarcely significant. As previously observed for H_{m0}^{maxAE}, also energy periods associated with the greatest fraction of the wave energy (T_{m0}^{maxAE}) have a null trend in most of the Mediterranean basin (Fig. 3,d), with isolated points showing negative or positive, scarcely significant, trends. Overall, trends of annual maxima are characterized by higher magnitude, as confirmed in De Leo et al. (2021a). Moreover, the divergence of the trend between mean and extreme wave conditions observed by Lobeto et al. (2021), at the global scale is evident also from the analysis at the Mediterranean basin scale performed in the present work.

As far as the annual mean values of specific wave power, P_{wave}^{mean}, is concerned (Fig. 4), increasing trends, highly significant, are observed in the Alborean Sea, along most of the western coast of Italy and the Aegen coasts of Croatia, Grece and Albania. In such areas, maximum s-values of around 0.01 kW/m per year are detected. Significant decreasing trends characterize, instead, the eastern Levantine Sea. It is worth noting that the detected trends on the mean annual wave power P_{wave}^{mean} are, overall, more significant over wider homogeneous geographical areas compared to those observed on annual mean values of significant wave height H_{m0}^{mean}.

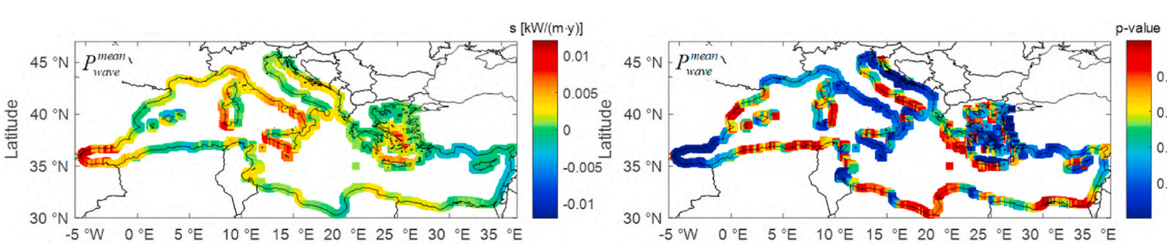

Fig. 4. Spatial distribution of Theil-Sen's slope *s* (left) and *p*-value of Mann-Kandall tests (right) in the IPCC's RCP8.5 scenario for the annual mean value of specific wave power P_{wave}^{mean}.

3.2. Optimal sizing and performance of the OWC in the present scenario

Considering the wave conditions of the present scenario, the optimal sizing (in terms of values of D, W and K) and the pneumatic AEP of OWCs along all the Mediterranean 20 m depth-contour are reported in Fig. 5 and Fig. 6. As aforementioned, the MRM is applied on pairs of H_{m0} and $T_{m\text{-}1,0}$ in each local SM by limiting the maximum wave height to values between 1 m and 5.5 m, assumed as representative of safe operative conditions for the device. Moreover, the model is applied considering wave periods in the range 4.4–9.2 s, to respect the applicability limits intrinsic in its formulation. Applying the MRM within this range allows considering pairs of H_{m0}, $T_{m\text{-}1,0}$ covering from 70% to 97% of the total annual energy AE in each geographical location.

The optimal chamber length W_{opt} varies between 7 m and 11 m (Fig. 5,a). W_{opt} has the lower values in the Adriatic Sea and the Aegean Sea, while the higher values are on the west coast of Sardinia and Corse and the north African coasts of Algeria and Tunisia. The spatial distribution of the optimal OWC chamber length W directly reflects that of the wavelength λ transporting the higher fraction of the wave energy in the installation site: indeed, optimal performances of the OWC for $W/\lambda \sim 0.12$ were previously found in the literature (e.g. Simonetti et al., 2017). The optimal geometry has a larger value of W_{opt} in locations where a higher fraction of the total wave energy, on a multi-annual basis, is transported by longer waves, as discussed later in this section comparing the wave climate of selected geographical locations.

The optimal damping applied on the OWC caisson by the PTO, K_{opt}, is strongly correlated to W_{opt} (Fig. 5,b): the lower the value of W_{opt}, the higher the value of K_{opt}. This effect is confirmed, and discussed in-depth, in previous works on OWC performance (e.g. in Simonetti et al. (2017) and Curran et al. (1997)). K_{opt} has values between 0.9 and 1.1 $kg^{1/2}m^{-7/2}$ over large areas of the Mediterranean basin, reaching maximum values of 1.3–1.4 $kg^{1/2}m^{-7/2}$ in the Adriatic and Aegean Seas and in some isolated spots as the Gulf of Gabès.

As discussed in Simonetti et al. (2017), D influences both the resonance frequency of the OWC chamber and the magnitude of the dynamic wave pressure acting at the level of the submerged front wall draft. Moreover, in highly energetic sea states, limited values of D may determine the occurrence of inlet broaching phenomena, penalizing the performance of the device. As a balance of the aforementioned factors, in the present study, an optimal value of D of around 3.5 m is found for most of the Mediterranean basin (Fig. 5,c). The D_{opt} increases to around 4 m along the western coast of Sardinia, in the Balearic Islands and in some locations along the North African coasts (attaining peaks of 4.7 m), i.e., where higher fractions of the annual wave energy are associated with higher waves compared to other locations in the Mediterranean basin.

The AEP of the device is considered in this work only with reference to the energy extracted in the primary conversion process, i.e. the pneumatic energy of the airflow directed towards the turbine. The spatial distribution of the specific pneumatic AEP (i.e. for unit width of the chamber perpendicular to the direction of wave propagation) achievable with the optimal OWC geometry (Fig. 6,a) reaches values up to 37 MWh/year·m, with maxima along the western coasts of Sardinia and Corse, that of Algeria and Tunisia and in the north of Balearic islands. Values of AEP around 15 MWh/year·m are found also in wide geographical areas along the North African coasts. Lower AEP values characterize the Adriatic and Aegean Seas, as a direct consequence of the lower availability of the wave energy resource (as shown in wave energy resource assessments available in the literature, e.g. in Besio et al. (2016).

Aiming to highlight locations more suitable for the installation of OWC devices, comprising also the economic point of view, the spatial distribution of the normalized LCOE of the optimal geometry is presented in (Fig. 6,b). Values of normalized LCOE lower than 0.1, denoting locations with the highest economic potential for the deployment of OWCs, are found in most of the 20 m bathymetric contours of the Mediterranean coasts of Africa, Balearic Islands, western sides of Corse, Sardinia and Sicily and in some areas in the central Italy. Favourable spots are also in some locations in the Aegean Sea. Adopting devices of optimized size allows to mitigate, in terms of LCOE, the significant differences observed in the spatial distribution of the AEP. The reasons are twofold: on the one hand, the optimization process allows maximizing the energy extracted in each installation site, on the other hand, the optimal OWC geometry, of reduced dimensions in less energetic sites, allows decreasing the CAPEX of the device, in turn decreasing the LCOE.

The SMs of the available wave resource in the present scenario, the extracted pneumatic energy, and the scatter of CW^* over different chamber lengths W and damping K are exemplarily shown for selected geographical locations in the Mediterranean Basin (P1-P5, Table 1 and Fig. 7). For P1, located in the north Tyrrhenian Sea, the application of the MRM, within the aforementioned applicability limits in terms of H_{m0} and $T_{m\text{-}1,0}$, allows evaluating the device performance for n pairs of H_{m0} and $T_{m\text{-}1,0}$ covering a considerable fraction of the total available wave energy AE in the scatter matrix (i.e. $\sum_n AE_n/AE = 0.95$, as reported in Table 1). In P1, the optimal configuration has W_{opt}=9.8 m, D_{opt}=3.9 m,

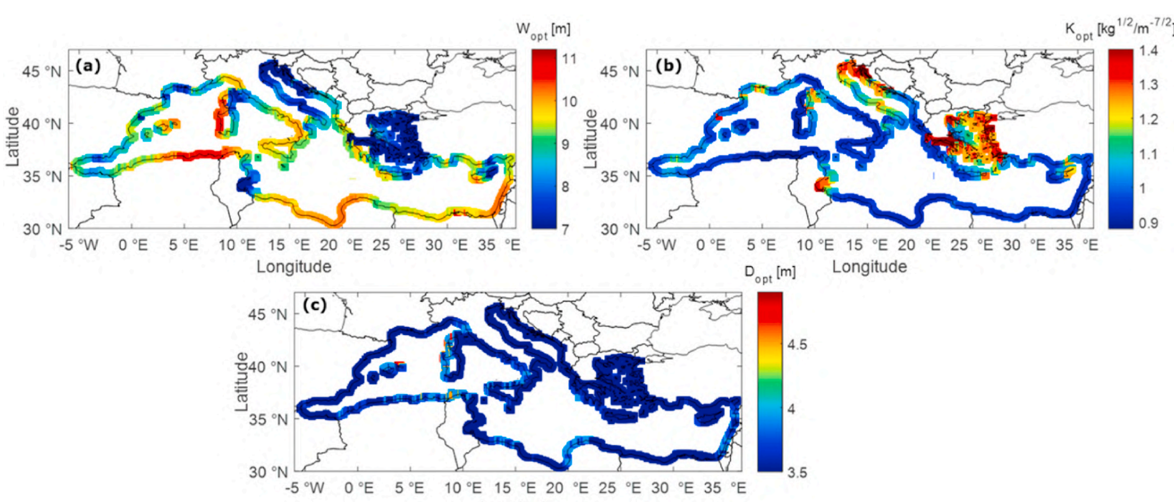

Fig. 5. Optimal values of: length of the OWC chamber, W_{opt} (a), damping applied by the PTO K_{opt} (b) and draft of the front wall D_{opt} (c). Results for the present wave climate scenario based on data from 1986 to 2016.

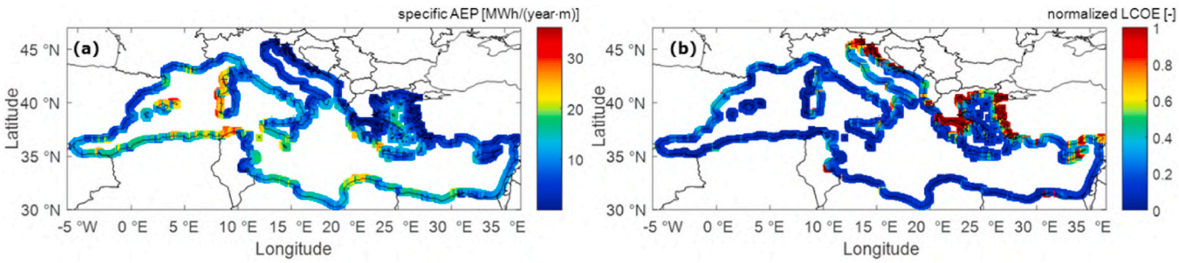

Fig. 6. Spatial distribution of the specific pneumatic Annual Energy Production (AEP) of the optimal OWC configuration (a) and normalized Levelized Cost of Energy (LCOE) (b) for the present wave climate scenario based on data from 1986 to 2016.

Table 1
Coordinates of the reference sites P1-P5 used for the detailed analysis, fraction of the total available annual energy (AE) in the reference site considered in the application of the MRM model, $\sum_n AE_n/AE$, optimal dimensions of the OWC, CW^* and AEP of the optimal geometry.

Marker	Coordinates	$\sum_n AE_n/AE$ [−]	W_{opt} [m]	K_{opt} [m]	D_{opt} [m]	CW* [−]	AEP [MWh/year·m]
P1	43.6°N, 10.2°E	0.95	9.8	0.92	3.9	0.54	12.35
P2	40.7°N, 8.1°E	0.93	10.4	0.92	4.7	0.50	35.89
P3	37.9°N, 12.3°E	0.92	9.4	0.96	3.7	0.54	19.55
P4	36.7°N, 5.3°E	0.81	10.8	0.88	3.5	0.52	11.68
P5	36.7°N, −3.2°W	0.92	7.8	1.08	3.5	0.54	6.46

Fig. 7. Location of the reference sites P1-P5 used for the detailed analysis in the Mediterranean Sea.

K_{opt}=0.92 kg$^{1/2}$m$^{-7/2}$, with an average capture with CW^*=0.54. For a fixed value of D=3.9 m, CW^* close to the maximum (i.e., CW^*>0.52) is obtained with values of W between 9.3 and 10.7 m, combined with K-values between 1.05 and 0.80 kg$^{1/2}$m$^{-7/2}$, respectively (Fig. 8,b). The pneumatic AEP achievable with the optimal geometry in P1 is estimated in around 12.35 MWh/year·m (Fig. 8,a). It is worth mentioning that SMs in Figs. 8–12,a are represented with 1 m and 1 s bins in H_{m0} and $T_{m-1,0}$ to increase the readability of the figure, while computations, as aforementioned, were carried out using a higher resolution of the bins (0.125 m and 0.125 s). The wave climate of P2, located in North Sardinia, is characterized by significantly higher AE (Fig. 9,a), which corresponds to a higher AEP (i.e. 35.9 MWh/year·m with the optimal geometry, i.e. W_{opt}=10.4 m, D_{opt}=4.7 m, K_{opt}= 0.92 kg$^{1/2}$m$^{-7/2}$, Fig. 9,b), obtained with CW^*= 0.50. In P3, located on the west Coast of Sicily Island, a similar value of CW^* *for* the optimized geometry (W_{opt}=9.4 m, D_{opt}=3.7 m, K_{opt}=0.96 kg$^{1/2}$m$^{-7/2}$, Fig. 10) allows to obtain a pneumatic AEP of around 20 MWh/year·m. The effect of the distribution of the wave energy among different pairs of H_{m0} and $T_{m-1,0}$ in the SM is evident if comparing the optimal values of the draft D obtained in P1, P2 and P3 (Figs. 8–10). In P2, waves with 4<H_{m0}<6 m transport 24% of the total wave energy in the local SM. In P1 and P3, this fraction decreases to 8.3% and 8.0%, respectively. Accordingly, a higher value of the optimal D (D_{opt}=4.7 m) is found for P2 compared to P1 (D_{opt}=3.9 m) and P3 (D_{opt}=3.7 m), reflecting the need to limit inlet broaching phenomena in the most energetic sea states. The relevance of the prevailing wavelength λ in determining the value of the optimal chamber length W_{opt} is evident comparing results in P4 and P5. In P4, situated along the coast of Algeria, 68% of the energy in the SM (Fig. 11,a) is transported by waves

Available AE [kWh/m·year]	$T_{m-1,0}$ [s]										
H_{m0} [m]	<3	3-4	4-5	5-6	6-7	7-8	8-9	9-10	10-11	11-12	> 12
8 - 9	0	0	0	0	0	0	0	0	0	0	43
7 - 8	0	0	0	0	0	0	0	0	41	33	25
6 - 7	0	0	0	0	0	0	0	13	82	8	9
5 - 6	0	0	0	0	0	0	4	194	254	44	0
4 - 5	0	0	0	0	0	5	659	1167	284	37	0
3 - 4	0	0	0	0	12	781	2638	954	169	17	0
2 - 3	0	0	1	47	1478	3497	2157	980	164	25	0
1 - 2	0	51	249	1522	3688	2422	2031	666	104	16	6
< 1	119	329	719	979	919	874	558	132	11	1	1

Extracted AE [kWh/m·year]	$T_{m-1,0}$ [s]										
H_{m0} [m]	<3	3-4	4-5	5-6	6-7	7-8	8-9	9-10	10-11	11-12	> 12
8 - 9	0	0	0	0	0	0	0	0	0	0	0
7 - 8	0	0	0	0	0	0	0	0	0	0	0
6 - 7	0	0	0	0	0	0	0	0	0	0	0
5 - 6	0	0	0	0	0	0	1	0	0	0	0
4 - 5	0	0	0	0	0	2	139	89	0	0	0
3 - 4	0	0	0	0	9	512	1280	168	0	0	0
2 - 3	0	0	0	25	1085	2362	1061	169	0	0	0
1 - 2	0	0	11	424	2342	1586	983	105	0	0	0
< 1	0	0	0	0	0	0	0	0	0	0	0

(a)

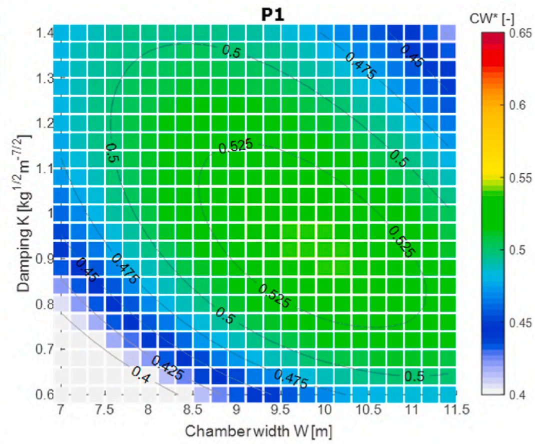

(b)

Fig. 8. Distribution of the available annual wave energy resource and of the pneumatic energy extracted by the optimal OWC geometry for point P1 (a); scatter plot of CW^{*} of the OWC device in the same location, for different W and K with D_{opt} = 3.9 m (b). Results refer to the present wave climate scenario.

Available AE [kWh/m·year]	$T_{m-1,0}$ [s]										
H_{m0} [m]	<3	3-4	4-5	5-6	6-7	7-8	8-9	9-10	10-11	11-12	> 12
8 - 9	0	0	0	0	0	0	0	0	0	331	14
7 - 8	0	0	0	0	0	0	0	9	215	644	80
6 - 7	0	0	0	0	0	0	0	226	1748	611	0
5 - 6	0	0	0	0	0	0	72	3878	3613	278	0
4 - 5	0	0	0	0	0	54	3161	9757	2020	63	0
3 - 4	0	0	0	0	49	2262	13599	6438	687	0	0
2 - 3	0	0	0	83	3222	10923	9585	1824	65	0	0
1 - 2	0	5	344	2697	7889	5135	1386	78	6	0	0
< 1	39	258	975	1559	774	98	11	1	0	0	0

Extracted AE [kWh/m·year]	$T_{m-1,0}$ [s]										
H_{m0} [m]	<3	3-4	4-5	5-6	6-7	7-8	8-9	9-10	10-11	11-12	> 12
8 - 9	0	0	0	0	0	0	0	0	0	0	0
7 - 8	0	0	0	0	0	0	0	0	0	0	0
6 - 7	0	0	0	0	0	0	0	0	0	0	0
5 - 6	0	0	0	0	0	0	10	58	0	0	0
4 - 5	0	0	0	0	0	34	1382	1379	0	0	0
3 - 4	0	0	0	0	35	1456	6667	1297	0	0	0
2 - 3	0	0	0	34	2150	7108	4960	428	0	0	0
1 - 2	0	0	7	491	4365	3284	731	17	0	0	0
< 1	0	0	0	0	0	0	0	0	0	0	0

(a)

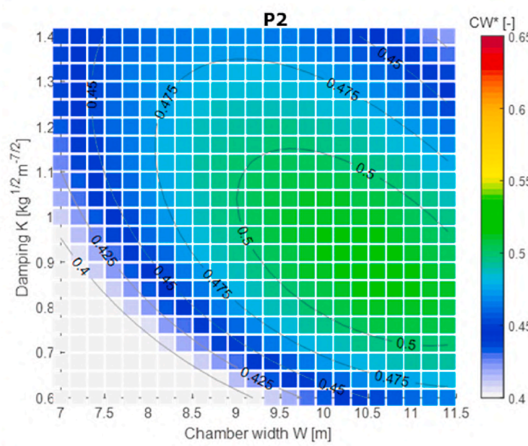

(b)

Fig. 9. Distribution of the available annual wave energy resource and of the pneumatic energy extracted by the optimal OWC geometry for point P2 (a); scatter plot of CW^{*} of the OWC device in the same location, for different W and K with D_{opt} = 4.7 m (b). Results refer to the present wave climate scenario.

Available AE [kWh/m·year]	$T_{m-1,0}$ [s]										
H_{m0} [m]	<3	3-4	4-5	5-6	6-7	7-8	8-9	9-10	10-11	11-12	> 12
8 - 9	0	0	0	0	0	0	0	0	0	0	118
7 - 8	0	0	0	0	0	0	0	0	0	23	62
6 - 7	0	0	0	0	0	0	0	27	130	91	28
5 - 6	0	0	0	0	0	0	53	197	401	207	57
4 - 5	0	0	0	0	0	43	448	1445	945	198	0
3 - 4	0	0	0	0	189	1135	3957	2578	610	132	0
2 - 3	0	0	0	360	2605	5276	4423	1304	394	31	27
1 - 2	0	43	1052	3492	6248	3514	1463	366	46	6	8
< 1	92	498	1166	1538	900	297	48	12	4	2	1

Extracted AE [kWh/m·year]	$T_{m-1,0}$ [s]										
H_{m0} [m]	<3	3-4	4-5	5-6	6-7	7-8	8-9	9-10	10-11	11-12	> 12
8 - 9	0	0	0	0	0	0	0	0	0	0	0
7 - 8	0	0	0	0	0	0	0	0	0	0	0
6 - 7	0	0	0	0	0	0	0	0	0	0	0
5 - 6	0	0	0	0	0	0	6	1	0	0	0
4 - 5	0	0	0	0	0	14	96	59	0	0	0
3 - 4	0	0	0	0	149	733	1700	337	0	0	0
2 - 3	0	0	0	199	1966	3546	2133	183	0	0	0
1 - 2	0	0	62	1105	4135	2357	708	63	0	0	0
< 1	0	0	0	0	0	0	0	0	0	0	0

(a)

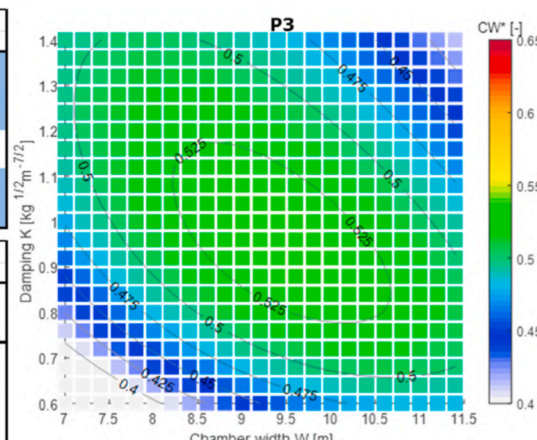

(b)

Fig. 10. Distribution of the available annual wave energy resource and of the pneumatic energy extracted by the optimal OWC geometry for point P3 (a); scatter plot of CW^{*} of the OWC device in the same location, for different W and K with D_{opt} = 3.7 m (b). Results refer to the present wave climate scenario.

Available AE [kWh/m·year]		$T_{m-1,0}$ [s]										
		<3	3-4	4-5	5-6	6-7	7-8	8-9	9-10	10-11	11-12	> 12
H_{m0} [m]	8 - 9	0	0	0	0	0	0	0	0	0	0	57
	7 - 8	0	0	0	0	0	0	0	0	0	0	287
	6 - 7	0	0	0	0	0	0	0	0	9	203	301
	5 - 6	0	0	0	0	0	0	0	0	415	835	75
	4 - 5	0	0	0	0	0	0	3	361	2311	882	29
	3 - 4	0	0	0	0	0	10	377	3174	3077	336	0
	2 - 3	0	0	1	1	55	818	4144	6114	934	73	6
	1 - 2	0	29	36	303	1903	5451	5649	989	127	33	1
	< 1	66	200	630	1392	2247	842	193	40	6	1	0

Extracted AE [kWh/m·year]		$T_{m-1,0}$ [s]										
		<3	3-4	4-5	5-6	6-7	7-8	8-9	9-10	10-11	11-12	> 12
H_{m0} [m]	8 - 9	0	0	0	0	0	0	0	0	0	0	0
	7 - 8	0	0	0	0	0	0	0	0	0	0	0
	6 - 7	0	0	0	0	0	0	0	0	0	0	0
	5 - 6	0	0	0	0	0	0	0	0	0	0	0
	4 - 5	0	0	0	0	0	0	1	5	0	0	0
	3 - 4	0	0	0	0	0	6	167	190	0	0	0
	2 - 3	0	0	0	1	38	523	1995	911	0	0	0
	1 - 2	0	0	1	87	1165	3460	2906	230	0	0	0
	< 1	0	0	0	0	0	0	0	0	0	0	0

(a)

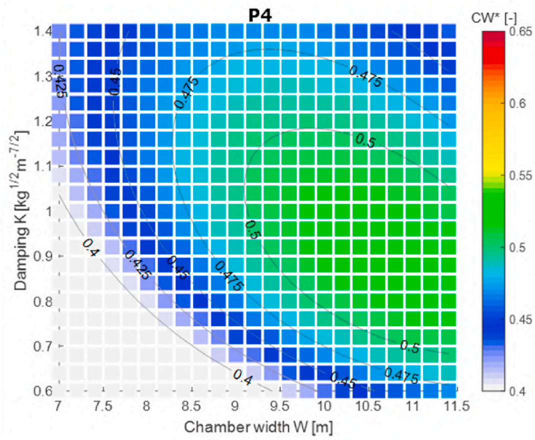

(b)

Fig. 11. Distribution of the available annual wave energy resource and of the pneumatic energy extracted by the optimal OWC geometry for point P4 (a); scatter plot of CW^* of the OWC device in the same location, for different W and K with $D_{opt} = 3.5$ m (b). Results refer to the present wave climate scenario.

Available AE [kWh/m·year]		$T_{m-1,0}$ [s]										
		<3	3-4	4-5	5-6	6-7	7-8	8-9	9-10	10-11	11-12	> 12
H_{m0} [m]	8 - 9	0	0	0	0	0	0	0	0	0	0	0
	7 - 8	0	0	0	0	0	0	0	0	0	0	0
	6 - 7	0	0	0	0	0	0	0	0	0	0	0
	5 - 6	0	0	0	0	0	0	0	9	10	0	0
	4 - 5	0	0	0	0	0	0	42	25	8	0	0
	3 - 4	0	0	0	0	8	179	203	22	0	0	2
	2 - 3	0	0	2	115	767	1071	364	57	19	0	0
	1 - 2	0	24	685	3294	3487	1015	223	26	0	0	0
	< 1	94	555	1495	1504	378	91	32	15	8	4	2

Extracted AE [kWh/m·year]		$T_{m-1,0}$ [s]										
		<3	3-4	4-5	5-6	6-7	7-8	8-9	9-10	10-11	11-12	> 12
H_{m0} [m]	8 - 9	0	0	0	0	0	0	0	0	0	0	0
	7 - 8	0	0	0	0	0	0	0	0	0	0	0
	6 - 7	0	0	0	0	0	0	0	0	0	0	0
	5 - 6	0	0	0	0	0	0	0	1	0	0	0
	4 - 5	0	0	0	0	0	0	7	1	0	0	0
	3 - 4	0	0	0	0	7	100	70	3	0	0	0
	2 - 3	0	0	1	73	608	692	154	5	0	0	0
	1 - 2	0	0	75	1233	2433	659	92	4	0	0	0
	< 1	0	0	0	0	0	0	0	0	0	0	0

(a)

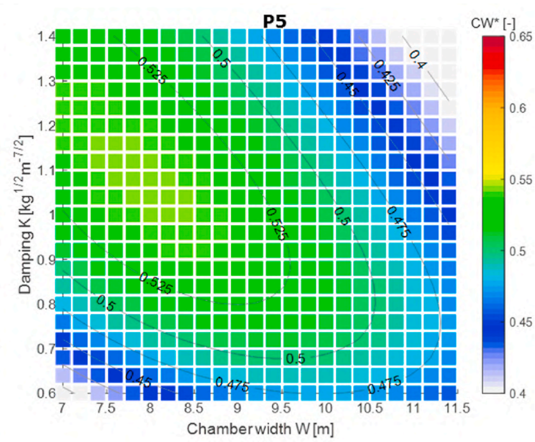

(b)

Fig. 12. Distribution of the available annual wave energy resource and of the pneumatic energy extracted by the optimal OWC geometry for point P5 (a); scatter plot of CW^* of the OWC device in the same location, for different W and K with $D_{opt} = 3.5$ m (b). Results refer to the present wave climate scenario.

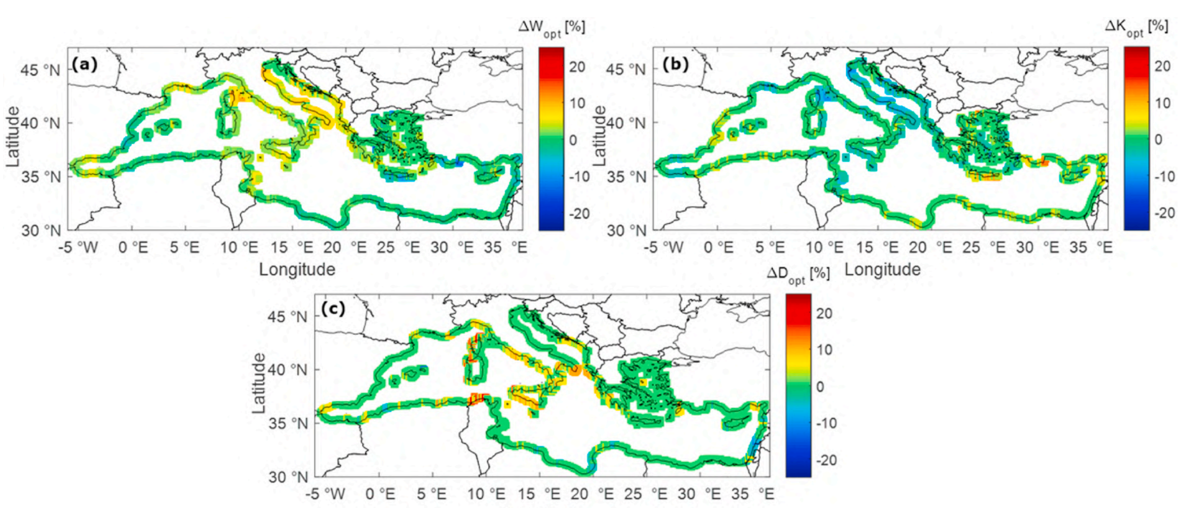

Fig. 13. Percentage variation of the optimal values of the OWC length W (a), damping K (b) and front wall draft D (c) between present (1986–2016) and projected future (2071–2100, with RCP8.5 emissions) scenarios.

with $T_{m-1,0}$>8 s. In the north Alboran Sean in P5 (Fig. 12), waves transporting most of the energy have significantly lower lengths, with 93% of the resource associated with waves with $T_{m-1,0}$<8 s (indeed, 78% of the AE in P5 corresponds to wave periods $T_{m-1,0}$<7 s). This difference reflects the greater values of W_{opt} predicted in P4 regarding P5, respectively 10.8 m and 7.8 m.

3.3. Effect of long-term trends in the wave climate on OWC sizing and performance

The MRM is applied to estimate the performance and optimal geometry of the OWC regarding the SMs obtained from the projected wave conditions for the period 2071–2100, under the RCP8.5 emission scenario. Comparing the results with those obtained for the present wave climate scenario, moderate variations are observed in the optimal chamber length W_{opt} (Fig. 13,a), which increases up to 10% in the Adriatic Sea and in the north Tyrrhenian Sea (in particular, between Corse and Tuscany). The increase of W_{opt} is lower than 10% in the Alboran Sea. On the contrary, relative decreases of W_{opt} up to −10% are observed in some spots in the Aegean Sea and on the Iberian coasts, in front of the Balearic Islands. Overall, variations are negligible over most of the Mediterranean Basin.

Among the different wave statistics, the highest level of correlation can be highlighted between locations showing increasing/decreasing trends in $T^{90th}_{m-1,0}$ and $T^{max}_{m-1,0}$ and those showing an increase/decrease in the optimal chamber length W_{opt}. Trends in the mean annual values of the energy period $T^{mean}_{m-1,0}$ (Fig. 3) appear, instead, to have a weaker correlation with variations of W_{opt}. It is worth noting that for the Spanish coast close to the Strait of Gibraltar, where trends in the annual values of $T^{90th}_{m-1,0}$ and $T^{max}_{m-1,0}$ are contrasting (with a significant increasing trend for $T^{90th}_{m-1,0}$ and an opposite decreasing trend, with low significance, for $T^{max}_{m-1,0}$ as shown in Fig. 3,b-c), the relative variation of W_{opt} is more limited compared to that between Corse and Tuscany (where both $T^{90th}_{m-1,0}$ and $T^{max}_{m-1,0}$ show increasing, significant trend).

Moderate variations (±10%) are observed also in the optimal damping level K_{opt} to be applied to the OWC chamber (Fig. 13,b). The spatial distribution the foreseen variation of K_{opt} matches closely that of W_{opt}: increasing optimal values of the chamber length W_{opt} generally correspond to decreasing values of K_{opt}, and vice versa.

Variations of the same order are found for the optimal value of the OWC draft D_{opt} (Fig. 13,c), with relative increases up to 10% near some coastal regions in the south of Italy and peaks up to 20% in some isolated spots in north Sardinia, Tunisia and Algeria. The limited variation of optimal OWC geometries is consistent with the absence of relevant trends on the wave periods and heights associated with the highest fraction of wave energy resource in each location, as discussed in *Section 3.1*.

The AEPs obtainable if the OWC geometries optimized for the period 1986–2016 are applied on the projected SM for the period 2071–2100 in RCP8.5 scenario considerably increases in most of the Mediterranean 20 m contours (Fig. 14,a). Maximum relative variations are found in the Adriatic Sea, along the Croatian coasts, and in the Aegean Sea around Peloponnese Peninsula, with the higher relative increases up to 75% in the Gulf of Corinth. The AEP also remarkably increases in the Alboran Sea and in central Italy (in the Tuscan Archipelago), where relative variations attain values of 40–50%. Negative relative variations, i.e. AEP values lower in the 2071–2100 scenario, are found for a few limited zones (i.e. south of Cyprus and part of the Gulf of Sidra). These negative variations are limited to less than −20%. Increases of AEP are due to an overall increase of the available wave energy resource in the future scenario (Fig. 4). As a direct consequence of the variation of the AEP, the LCOE would decrease over most of the 20 m contours in the Mediterranean Basin, with projected values up to −25% lower (e.g. along Spanish, French and Italian coasts, as well as in some Adriatic and Aegean locations) (Fig. 14,b). The AEP shows no relative variation in front of the north African coast of Algeria and Tunisia, as well as in the western side of Corse and Sardinia, i.e. in regions characterized, in the present scenario, by the higher values of wave energy flux in the Mediterranean basin, as unanimously shown in the literature, e.g. in Besio et al. (2016); Liberti et al. (2013); Vannucchi and Cappietti (2016).

It is worth mentioning that the differences in AEP and LCOE estimated on the SMs of the scenario 2071–2100 would be negligible (i.e., <± 5%) if using OWC geometries specifically optimized with reference to the wave climate of the future scenario, instead of that optimized on the SMs relative to 1986–2016.

The SMs of the available wave resource in the future scenario, the AEP obtained with the optimal geometry and the scatter of CW^* over different chamber lengths W and dampings K for points P1-P5 (defined in Table 1 and Fig. 7) are reported in Appendix II.

4. Discussion

In the present work, an approach based on SM is used to represent sea states and to estimate the OWC device performance by applying the MRM proposed by Simonetti et al. (2018a). In this approach, sea states are represented considering only a pair of wave parameters (i.e., significant wave height H_{m0} and energy period $T_{m-1,0}$). The shortcomings of this approach were discussed in Mérigaud and Ringwood (2018). The authors concluded that SM-based representations of the sea state and of the related WEC performance may introduce inaccuracy in the estimation of the power production of WECs, especially for locations where wave spectra significantly differ from standard shapes. The effect of the degree of fidelity in representing wave and environmental conditions (i.e., assessment of power production and performance based on two-parameters SM, or more sophisticated environmental representations) was also discussed by Robertson et al. (2019). The authors proved that an assessment based on full environmental representation (including wind, tidal currents and considering spectral width and directional spreading to characterize waves) could reduce the estimated mean power production by 11.6% compared to assessments based on SMs in which wave heights and periods are divided into 0.5 m and 1 s

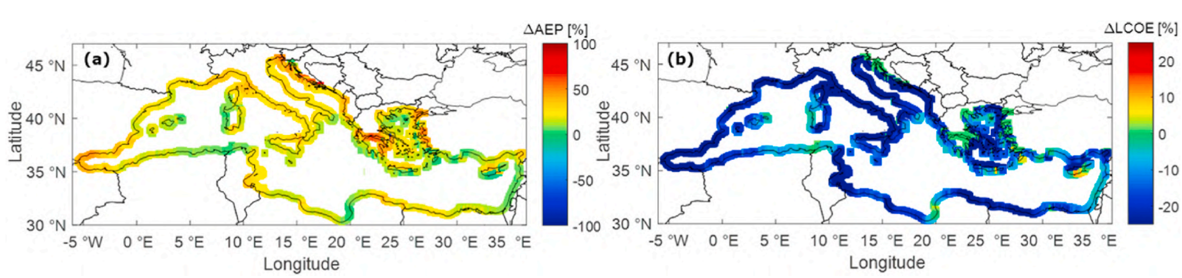

Fig. 14. Percentage variation of AEP (a) and LCOE (b) of OWCs between present (1986–2016) and future (2071–2100, with RCP8.5 emissions) scenarios. Results are relative to the performance of the optimal OWC geometry determined for the present scenario, applied alternatively on both the scatter matrices SMs of the present the future scenarios.

bins. To partially overcome this limitation, a higher resolution was adopted in the present work to discretize the SM for the application of the MRM, using bins of 0.125 s and 0.125 m for wave heights and wave periods. However, using a two-parameters SM-based approach in representing sea states was fundamental to allow assessing the OWC performance for a vast number of geometry alternatives over the whole 20 m water depth-contour in the Mediterranean Basin, as needed to perform an optimization study, maintaining a feasible computational time. Furthermore, in the present work the strong assumption of standard spectral shape is used to obtain the energy period $T_{m-1,0}$ from the only available data in the CDS-C3S of Copernicus, i.e. the peak period. The authors recognize that this assumption may introduce some inaccuracies in the estimation of the device performance. These inaccuracies are, however, considered acceptable for the present study, which primarily aims at providing preliminary information on the optimal sizing of OWC devices in different geographical locations and on the relative differences expected in the projected climate change scenarios. An assessment of spectral shape variations in climate change scenarios, and the consequent effect induced by such variations on WECs productivity should be evaluated in future research works.

This work, in line with most of the published literature (Mentaschi et al., 2017), considers projected change in annual average conditions, as well as in high percentile values and annual maxima. Possible large-scale variations in extreme events with a high return period are not considered. It is recognized that the impact of extreme events on the overall power production of WECs and, even more relevantly, on their survivability, with related implications for the engineering design process, should be carefully considered in future studies. Possible variations in the wave direction are not analysed as well.

The use of the MRM allows to include the effect of nonlinear phenomena observed in the dataset used for the model formulation. However, since the MRM is formulated based on multiple regression, its applicability is bound to the prescribed formulation range, limiting the geometric configurations of the device which can be studied. However, in the application of the MRM in this work it is possible to clearly identify an optimal geometry configuration in all the geographical locations considered. This suggests that the range of parameters used is adequate. Moreover, being formulated on laboratory tests and CFD numerical modelling at small scale, i.e. in a context where air-compressibility spring like effects are not properly reproduced, the model represents incompressible flow conditions (Falcão and Henriques, 2014). For OWC devices with similar geometry characteristics to those studied in the present work, the magnitude of the error induced by this approximation on the prediction of CW^* was found to be lower than 10% (Simonetti et al., 2018b). Moreover, the impact of considering air compressibility was assessed to be irrelevant for the selection of the optimal OWC geometry in a previous work by the Authors (Simonetti and Cappietti, 2019): the optimal design parameters selected for the OWC would be the same whether air compressibility is considered or not. Further limitations of the present work arise from the fact that the MRM has been formulated based on a dataset of CW^* obtained under regular and orthogonal wave attacks, possibly introducing some inaccuracies in the predicted performance under irregular and inclined waves. Considering the relatively shallow water depth used for the application in this work, it is assumed that, due to refraction, the ray of each wave of the local wave climate is already almost orthogonal to the 20 m depth contour, i.e. in turn parallel to the OWC's frontal wall. Therefore, the approximation derived by the application of the MRM is deemed acceptable, at least to the limit of validity of such a hypothesis.

Maximum values of the AEP obtained in this study, for the present scenario, are of the order of 37 MWh/m·year, for western Sardinia, Corse and Algeria. Such values are consistent with available data in the literature. In this respect, it is worth mentioning that the AEP obtainable with the optimal OWC configuration for a hypothetical installation along the Tyrrhenian coasts in central Italy, for a total length of the plant of 1 km, would be estimated in around $12 \cdot 10^3$ MWh/year (Fig. 6,a). Hypnotizing a global efficiency of the secondary and tertiary conversion processes of around 0.5, this value would be of the same order of the estimated electrical energy produced in a year from a REWEC3 plant with a total length of 1 km near Civitavecchia, i.e. 6-$9 \cdot 10^3$ MWh/year (Arena et al., 2017; Mattiazzo, 2019).

Finally, it should be mentioned that, in the present work, the PTO system is optimized only in terms of the ideal damping which should be applied on the OWC caisson. The possibility to design and manufacture air turbines capable of operating at such damping levels, while maintaining satisfactory performance, should be addressed in future works.

5. Conclusions

The optimal geometry and damping applied by the PTO for fixed, bottom-detached, asymmetric and rectangular-shaped OWC devices are evaluated along the whole 20 m water-depth contour of the Mediterranean basin, comparing results obtained under wave conditions representative of the present scenario to those obtained under waves projected to 2100 by the Climate Data Store of the Copernicus Climate Change Service. The empirical model proposed in Simonetti et al. (2018a), is used to evaluate the capture width ratio of the OWC. The model provides a compromise between high-fidelity and more simplified modelling approaches, allowing to compare a vast number of design alternatives of the OWC with limited computational cost.

Concerning the projection of significant wave height H_{m0}, positive trends, significant but limited in magnitude, are observed in the Alboran Sea close to the Strait of Gibraltar for annual mean values, 90th percentile and annual maxima of H_{m0}. Decreasing trends of the mean and 90th percentile of H_{m0} are found in some locations in the north Africa and the eastern Levantine Sea. The divergence of the trend between mean and extreme wave conditions observed at the global scale in the literature (Lobeto et al., 2021) is evident also at the Mediterranean basin scale, particularly when considering different statistics of the wave period: negative and significant trends on $T_{m-1,0}^{mean}$ are observed, e.g., on the western coasts of Corse and Sardinia, on the north of Sicily and in the Eastern Ionian Sea close to Greece and Albania. In the same geographical areas, negative trends are not observed, instead, when considering higher percentiles of $T_{m-1,0}$ or annual maxima. In the Alboran Sea close to the Strait of Gibraltar, $T_{m-1,0}^{max}$ shows a decreasing trend, while $T_{m-1,0}^{mean}$ and $T_{m-1,0}^{90th}$ in the same zone show an opposite increasing trend. In general, trends of annual maxima are more geographically dispersed compared to lower percentiles or mean values, but they are characterized by higher magnitude. As far as the wave energy resource is concerned, increasing trends with a high level of significance are detected in the mean annual value of wave power in the Alborean Sea, along most of the western coast of Italy and the Aegen coasts of Croatia, Grece and Albania.

The best-performing geometry of the OWC is found to vary significantly across the different geographical locations, with maximum values of the chamber length (W~11 m) along the north African coasts and the west coasts of Sardinia and Corse, i.e. in locations where a greater fraction of the wave energy is associated with longer waves. The minimum optimal value of chamber length is found in the Adriatic and Aegean Seas (W~7 m). Correspondingly, lower optimal values of damping were found in combination with higher chamber lengths, and vice-versa. A relative comparison of the LCOE among different geographical locations allowed identifying spots with the higher economic potential for installing OWCs, i.e. most of the north African coast, the Balearic Islands, western sides of Corse, Sardinia and Sicily and some areas in central Italy. Favourable spots are also found in the Aegean Sea, where the smaller size of the optimal device (which in turn reduces the construction costs) allows to compensate for the lower available wave resource.

Considering the more pessimistic emission scenario (RCP8.5), the long-term change in the wave energy resource results in moderate modifications of the optimal geometry of the OWC, with relative variations of dimensions between the present and the projected future scenario up to 10%. A high correlation is found between locations showing increasing or decreasing trends in $T^{max}_{m-1,0}$ and $T^{90th}_{m-1,0}$ and those showing corresponding variations in the optimal OWC chamber length. In the future wave climate scenario, the AEP of the OWC would significantly increase in most of the Mediterranean 20 m water-depth contours, attaining variations of 75% in some locations in the Aegean Sea and up to 50% in the Alboran Sea. These variations would result in a decrease of LCOE, in turn potentially increasing the commercial competitiveness of the OWC technology from an economic point of view.

CRediT authorship contribution statement

Irene Simonetti: Conceptualization, Methodology, Formal analysis, Investigation, Data curation, Writing – original draft, Writing – review & editing. **Lorenzo Cappietti:** Conceptualization, Methodology, Formal analysis, Investigation, Data curation, Writing – original draft, Writing – review & editing.

Declaration of competing interest

The authors declare that they have no known competing financial interests or personal relationships that could have appeared to influence the work reported in this paper.

Data availability

Data will be made available on request.

Nomenclature

Symbols

AE_n	Annual energy associated to the n-th pair of H_{m0}, $T_{m-1,0}$ in the SM [kWh/m]
B	OWC chamber length, perpendicular to wave propagation direction [m]
c_g	group velocity for surface waves [m/s]
CW^*	capture width ratio of the OWC [−]
CW^*_n	Capture width associated to the n-th pair of H_{m0}, $T_{m-1,0}$ in the SM [−]
D	Draft of the OWC front wall [−]
Fb	OWC chamber freeboard [m]
G	Length of the OWC lateral and back walls [m]
g	gravitational acceleration [m/s^2]
$Hm0$	significant wave height [m]
h	water depth [m]
j	weighted average cost of capital [%]
K	Quadratic damping applied by the PTO on the OWC chamber [kg$^{1/2}$m$^{-7/2}$]
k	wave number [1/m]
kh	relative water depth [−]
m	lifetime of the project [years]
p	*p*-value of Mann-Kandall tests [−]
P_{owc}	wave energy extracted by the OWC device in the form of pneumatic energy [kW/m]
P_{wave}	energy of the incident wave [kW/m]
s	Theil-Sen's slope [unit/year]
$T_{m-1,0}$	energy period [s]
W	OWC chamber width in wave propagation direction [m]
α	Correlation factor between energy and peak period [−]
γ	peach enhancement factor of JONSWAP spectrum [−]
λ	wavelength of sea waves [m]
ρ	water density [kg/m^3]
ρ_a	air density [kg/m^3]

Abbreviations

AE	Annual Energy associated to the local wave resource
AEP	Annual Energy Production of the OWC
C3S	Copernicus Climate Change Service
CAPEX	Capital expenditure
CDS	Copernicus Data Store
ECMWF	European Centre of Medium-range Weather Forecast
GHG	Greenhouse Gasses
IPCC	Intergovernmental Panel for Climate Change
LCOE	Levelized Cost Of Energy
MRM	Multiple Regression Model
OPEX	Operational Expenditure
OWC	Oscillating Water Column
PTO	Power Take Off
RCP	Representative Concentration Pathway
SM	Scatter Matrix of annual wave energy
WEC	Wave Energy Converters

Appendix I

The parameters, functions and numerical coefficients constituting the MRM proposed by the Authors in (Simonetti et al., 2018a) are reported in Equations AI.1-AI.9 and in Table AI.1. The applicability limits of the model are as follows: $h^* = 1.5–3.5$, $D^* = 1.8–5$, $W^* = 0.08–0.2$, $K^* = 20–170$. The reader is referred to the original paper for details on the model derivation.

$$h^* = kh \tag{AI.1}$$

$$D^* = D \Big/ \left(H \cdot \frac{\cosh k(h - D)}{\cosh(kh)}\right) \tag{AI.2}$$

$$W^* = W/_{\lambda} \tag{AI.3}$$

$$K^* = K \cdot B \cdot W / \rho_a^{1/2} \tag{AI.4}$$

$$f_1(K^* - d) = \frac{(P_1 \cdot (K^* - d) + P_2)}{\left((K^* - d)^2 + Q_1 \cdot (K^* - d) + Q_2\right)} \tag{AI.5}$$

$$a(h^*) = \frac{(P_3 \cdot h^* + P_4)}{(h^{*2} + Q_3 \cdot h^* + Q_4)} \tag{AI.6}$$

$$b(h^*) = P_5 \cdot h^{*2} + P_6 \cdot h^* + P_7 \tag{AI.7}$$

$$c(h^*) = P_8 h^{*P_9} + P_{10} \tag{AI.8}$$

$$d\left(h^*\right) = P_{11} h^{*3} + P_{12} h^{*2} + P_{13} h^* + P_{14} \tag{AI.9}$$

$$CW^* = \frac{f_1(K^* - d(h^*))}{exp(a(h^*)D^*) \cdot 1 + \left(W^* - W^*_{opt}\right)^2 \cdot b(h^*) \cdot c(h^*)} \tag{AI.10}$$

Table AI. 1
numerical coefficient of the MRM proposed in (Simonetti et al., 2018a).

Numerical coefficients			
$P_1 = 145$	$P_2 = 39.6$	$Q_1 = -23.1$	$Q_2 = 6300$
$P_3 = 0.133$	$P_4 = -0.18$	$Q_3 = -5.38$	$Q_4 = 8.02$
$P_5 = 117.1$	$P_6 = -581.3$	$P_7 = 748.9$	
$P_8 = 3.08$	$P_9 = -2.68$	$P_{10} = 0.58$	
$P_{11} = -6.68$	$P_{12} = 67.6$	$P_{13} = -196.4$	$P_{14} = 176.4$

Appendix II

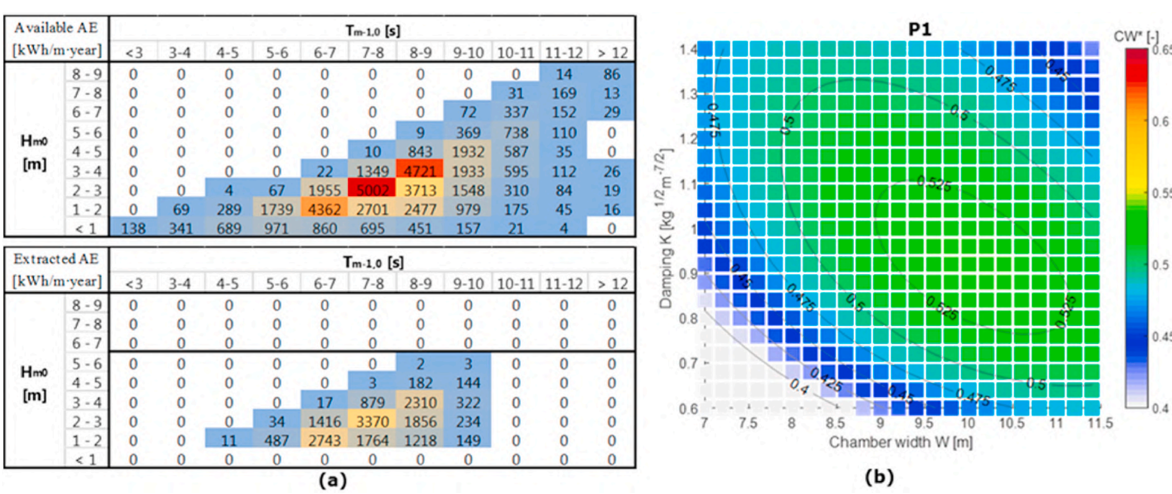

Available AE [kWh/m·year] — H_{m0} [m]	$T_{m-1,0}$ [s] <3	3-4	4-5	5-6	6-7	7-8	8-9	9-10	10-11	11-12	> 12
8 - 9	0	0	0	0	0	0	0	0	0	14	86
7 - 8	0	0	0	0	0	0	0	0	31	169	13
6 - 7	0	0	0	0	0	0	0	72	337	152	29
5 - 6	0	0	0	0	0	0	9	369	738	110	0
4 - 5	0	0	0	0	0	10	843	1932	587	35	0
3 - 4	0	0	0	0	22	1349	4721	1933	595	112	26
2 - 3	0	0	4	67	1955	5002	3713	1548	310	84	19
1 - 2	0	69	289	1739	4362	2701	2477	979	175	45	16
< 1	138	341	689	971	860	695	451	157	21	4	0

Extracted AE [kWh/m·year] — H_{m0} [m]	$T_{m-1,0}$ [s] <3	3-4	4-5	5-6	6-7	7-8	8-9	9-10	10-11	11-12	> 12
8 - 9	0	0	0	0	0	0	0	0	0	0	0
7 - 8	0	0	0	0	0	0	0	0	0	0	0
6 - 7	0	0	0	0	0	0	0	0	0	0	0
5 - 6	0	0	0	0	0	0	2	3	0	0	0
4 - 5	0	0	0	0	0	3	182	144	0	0	0
3 - 4	0	0	0	0	17	879	2310	322	0	0	0
2 - 3	0	0	0	34	1416	3370	1856	234	0	0	0
1 - 2	0	0	11	487	2743	1764	1218	149	0	0	0
< 1	0	0	0	0	0	0	0	0	0	0	0

Fig. AII. 1. Distribution of the available annual wave energy resource and of the pneumatic energy extracted by the optimal OWC geometry for point P1 (a); scatter plot of CW^* of the OWC device in the same location, for different W and K with $Dopt = 3.9$ m (b). Results refer to the projected wave climate for 2071–2100 under RCP8.5 emission scenario.

Available AE [kWh/m·year]	$T_{m-1,0}$ [s]										
H_{m0} [m]	<3	3-4	4-5	5-6	6-7	7-8	8-9	9-10	10-11	11-12	> 12
8 - 9	0	0	0	0	0	0	0	0	0	331	14
7 - 8	0	0	0	0	0	0	0	9	215	644	80
6 - 7	0	0	0	0	0	0	0	226	1748	611	0
5 - 6	0	0	0	0	0	0	72	3878	3613	278	0
4 - 5	0	0	0	0	0	54	3161	9757	2020	63	0
3 - 4	0	0	0	0	49	2262	13599	6438	687	0	0
2 - 3	0	0	0	83	3222	10923	9585	1824	65	0	0
1 - 2	0	5	344	2697	7889	5135	1386	78	6	0	0
< 1	39	258	975	1559	774	98	11	1	0	0	0

Extracted AE [kWh/m·year]	$T_{m-1,0}$ [s]										
H_{m0} [m]	<3	3-4	4-5	5-6	6-7	7-8	8-9	9-10	10-11	11-12	> 12
8 - 9	0	0	0	0	0	0	0	0	0	0	0
7 - 8	0	0	0	0	0	0	0	0	0	0	0
6 - 7	0	0	0	0	0	0	0	0	0	0	0
5 - 6	0	0	0	0	0	0	10	58	0	0	0
4 - 5	0	0	0	0	0	34	1382	1379	0	0	0
3 - 4	0	0	0	0	35	1456	6667	1297	0	0	0
2 - 3	0	0	0	34	2150	7108	4960	428	0	0	0
1 - 2	0	0	7	491	4365	3284	731	17	0	0	0
< 1	0	0	0	0	0	0	0	0	0	0	0

(a)

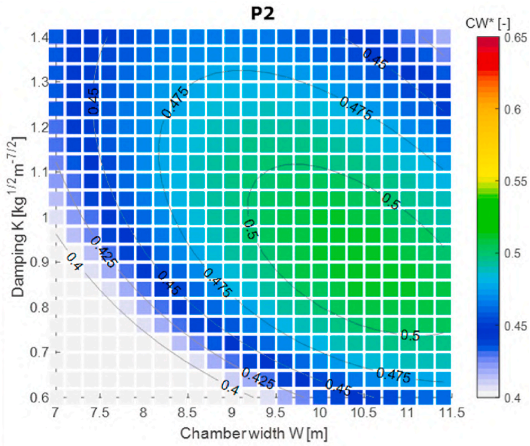

Fig. AII. 2. Distribution of the available annual wave energy resource and of the pneumatic energy extracted by the optimal OWC geometry for point P2 (a); scatter plot of CW^* of the OWC device in the same location, for different W and K with $Dopt = 4.9$ m (b). Results refer to the projected wave climate for 2071–2100 under RCP8.5 emission scenario.

Available AE [kWh/m·year]	$T_{m-1,0}$ [s]										
H_{m0} [m]	<3	3-4	4-5	5-6	6-7	7-8	8-9	9-10	10-11	11-12	> 12
8 - 9	0	0	0	0	0	0	0	0	72	15	31
7 - 8	0	0	0	0	0	0	0	10	84	144	219
6 - 7	0	0	0	0	0	0	0	82	472	515	280
5 - 6	0	0	0	0	0	4	84	469	1310	535	258
4 - 5	0	0	0	0	2	211	933	3250	1995	423	184
3 - 4	0	0	0	1	334	1498	5467	4336	966	194	48
2 - 3	0	0	3	616	2909	6272	5603	1549	409	73	14
1 - 2	0	57	1313	3719	5985	3571	1384	390	48	14	2
< 1	107	544	1139	1471	773	210	52	15	1	1	0

Extracted AE [kWh/m·year]	$T_{m-1,0}$ [s]										
H_{m0} [m]	<3	3-4	4-5	5-6	6-7	7-8	8-9	9-10	10-11	11-12	> 12
8 - 9	0	0	0	0	0	0	0	0	0	0	0
7 - 8	0	0	0	0	0	0	0	0	0	0	0
6 - 7	0	0	0	0	0	0	0	0	0	0	0
5 - 6	0	0	0	0	0	1	6	5	0	0	0
4 - 5	0	0	0	0	1	68	211	117	0	0	0
3 - 4	0	0	0	1	259	1002	2508	586	0	0	0
2 - 3	0	0	0	307	2128	4203	2749	220	0	0	0
1 - 2	0	0	62	1018	3787	2378	686	63	0	0	0
< 1	0	0	0	0	0	0	0	0	0	0	0

(a)

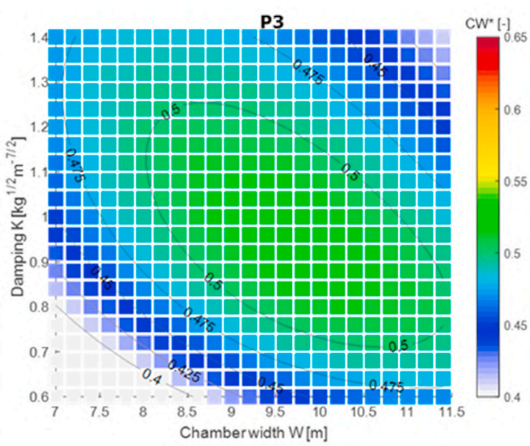

Fig. AII. 3. Distribution of the available annual wave energy resource and of the pneumatic energy extracted by the optimal OWC geometry for point P3 (a); scatter plot of CW^* of the OWC device in the same location, for different W and K with $Dopt = 3.9$ m (b). Results refer to the projected wave climate for 2071–2100 under RCP8.5 emission scenario.

Available AE [kWh/m·year]	$T_{m-1,0}$ [s]										
H_{m0} [m]	<3	3-4	4-5	5-6	6-7	7-8	8-9	9-10	10-11	11-12	> 12
8 - 9	0	0	0	0	0	0	0	0	0	0	47
7 - 8	0	0	0	0	0	0	0	0	0	23	349
6 - 7	0	0	0	0	0	0	0	0	38	189	466
5 - 6	0	0	0	0	0	0	0	5	418	1184	422
4 - 5	0	0	0	0	0	0	3	485	2284	1242	128
3 - 4	0	0	0	0	0	20	617	3635	3618	540	39
2 - 3	0	0	0	0	72	880	4434	6102	1275	71	30
1 - 2	0	53	86	541	2327	5574	5527	1196	147	42	18
< 1	71	246	828	1556	2195	757	192	33	7	3	0

Extracted AE [kWh/m·year]	$T_{m-1,0}$ [s]										
H_{m0} [m]	<3	3-4	4-5	5-6	6-7	7-8	8-9	9-10	10-11	11-12	> 12
8 - 9	0	0	0	0	0	0	0	0	0	0	0
7 - 8	0	0	0	0	0	0	0	0	0	0	0
6 - 7	0	0	0	0	0	0	0	0	0	0	0
5 - 6	0	0	0	0	0	0	0	0	0	0	0
4 - 5	0	0	0	0	0	0	1	4	0	0	0
3 - 4	0	0	0	0	0	12	261	224	0	0	0
2 - 3	0	0	0	0	50	563	2145	891	0	0	0
1 - 2	0	0	3	151	1417	3542	2845	265	0	0	0
< 1	0	0	0	0	0	0	0	0	0	0	0

(a)

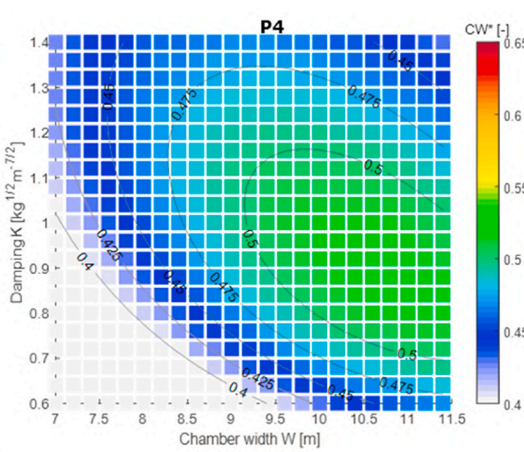

Fig. AII. 4. Distribution of the available annual wave energy resource and of the pneumatic energy extracted by the optimal OWC geometry for point P4 (a); scatter plot of CW^* of the OWC device in the same location, for different W and K with $Dopt = 3.5$ m (b). Results refer to the projected wave climate for 2071–2100 under RCP8.5 emission scenario.

Available AE [kWh/m·year]	H_{m0} [m]	$T_{m-1,0}$ [s] <3	3-4	4-5	5-6	6-7	7-8	8-9	9-10	10-11	11-12	> 12
	8 - 9	0	0	0	0	0	0	0	0	0	0	0
	7 - 8	0	0	0	0	0	0	0	0	0	0	0
	6 - 7	0	0	0	0	0	0	0	0	0	0	0
	5 - 6	0	0	0	0	0	0	18	79	67	0	0
	4 - 5	0	0	0	0	0	10	169	134	32	14	0
	3 - 4	0	0	0	5	31	293	492	166	54	44	0
	2 - 3	0	0	1	237	1077	1753	794	147	28	4	0
	1 - 2	0	28	1044	4186	5029	2018	450	50	12	6	0
	< 1	84	547	1525	1534	380	111	34	12	2	1	3

Extracted AE [kWh/m·year]	H_{m0} [m]	$T_{m-1,0}$ [s] <3	3-4	4-5	5-6	6-7	7-8	8-9	9-10	10-11	11-12	> 12
	8 - 9	0	0	0	0	0	0	0	0	0	0	0
	7 - 8	0	0	0	0	0	0	0	0	0	0	0
	6 - 7	0	0	0	0	0	0	0	0	0	0	0
	5 - 6	0	0	0	0	0	0	3	3	0	0	0
	4 - 5	0	0	0	0	0	3	32	9	0	0	0
	3 - 4	0	0	0	4	26	160	162	14	0	0	0
	2 - 3	0	0	0	150	853	1147	345	18	0	0	0
	1 - 2	0	0	103	1542	3512	1326	197	9	0	0	0
	< 1	0	0	0	0	0	0	0	0	0	0	0

(a)

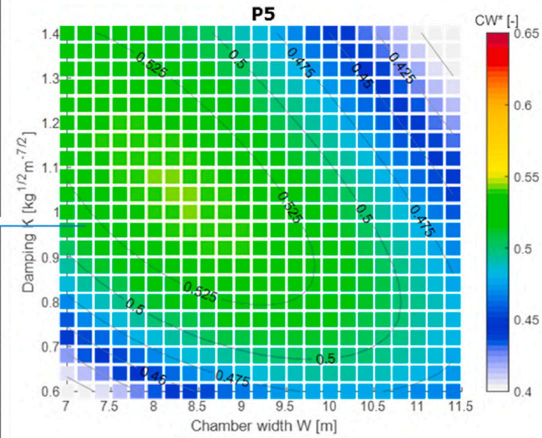

(b)

Fig. AII. 5. Distribution of the available annual wave energy resource and of the pneumatic energy extracted by the optimal OWC geometry for point P5 (a); scatter plot of CW^* of the OWC device in the same location, for different W and K with $Dopt = 3.5$ m (b). Results refer to the projected wave climate for 2071–2100 under RCP8.5 emission scenario.

References

de Andrés, A.D., Guanche, R., Weber, J., Costello, R., 2015. Finding gaps on power production assessment on WECs: wave definition analysis. Renew. Energy 83, 171–187. https://doi.org/10.1016/j.renene.2015.04.026. Nov.

de Andres, A., Maillet, J., Hals Todalshaug, J., Möller, P., Jeffrey, H., 2016. 'On the Optimum Sizing of a Real WEC from a Techno-Economic Perspective', Presented at the ASME 2016 35th International Conference on Ocean. Offshore and Arctic Engineering. https://doi.org/10.1115/OMAE2016-54110. Jun.

de Andres, A., Medina-Lopez, E., Crooks, D., Roberts, O., Jeffrey, H., 2017. On the reversed LCOE calculation: design constraints for wave energy commercialization. Int. J. Mar. Energy 18, 88–108. https://doi.org/10.1016/j.ijome.2017.03.008. Jun.

Ardhuin, F., et al., 2010. Semiempirical dissipation source functions for ocean waves. Part I: definition, Calibration, and validation. J. Phys. Oceanogr. 40 (9), 1917–1941. https://doi.org/10.1175/2010JPO4324.1. Sep.

Arena, F., Romolo, A., Malara, G., Fiamma, V., Laface, V., 2017. 'The First Full Operative U-OWC Plants in the Port of Civitavecchia', Presented at the ASME 2017 36th International Conference on Ocean. Offshore and Arctic Engineering. https://doi.org/10.1115/OMAE2017-62036. Jun.

Besio, G., Mentaschi, L., Mazzino, A., 2016. Wave energy resource assessment in the Mediterranean Sea on the basis of a 35-year hindcast. Energy 94, 50–63. https://doi.org/10.1016/j.energy.2015.10.044. Jan.

Caires, S., Yan, K., 2022. Ocean surface wave time series for the European coast from 1976 to 2100 derived from climate projections. (Accessed on Feb. 2022) DOI: 10.24381/cds.572bf382. Copernicus Climate Change Service (C3S) Climate Data Store (CDS). Feb.

Chozas, J.F., 2015. International Levelised Cost of Energy for Ocean Energy Technology - Cost of Ocean Energy: Energy Cost Analysis and Forecasts for Ocean Energy Converters. OES - OIEA. : Mar. 09, 2022. [Online]. Available: https://www.ocean-energy-systems.org/documents/16823-international-levelised-cost-of-energy-for-ocean-energy-technologies-2015-may-2015.pdf/.

Ciappi, L., et al., 2022. Wave-to-wire models of wells and impulse turbines for oscillating water column wave energy converters operating in the Mediterranean Sea. Energy 238, 121585. https://doi.org/10.1016/j.energy.2021.121585. Jan.

Curran, R., Stewart, T.P., Whittaker, T.J.T., 1997. Design synthesis of oscillating water column wave energy converters: performance matching. Proc. Inst. Mech. Eng. Part J. Power Energy 211 (6), 489–505. https://doi.org/10.1243/0957650981537375. Sep.

ECMWF, 2019. Product User Guide for Sea Level and Ocean Wave Products - Time Series and Indicators - C3S_422_Lot2_Deltares - European Services, Official Reference Number Service Contract: 2019/C3S_422_Lot2_Deltares/SC2,. Copernicus Climate Change Service. http://datastore.copernicus-climate.eu/documents/sis-european-coasts/Product_user_guide_sea_level_wave_v4_final.pdf, 2019.

Falcão, A.F.O., 2004. Stochastic modelling in wave power-equipment optimization: maximum energy production versus maximum profit. Ocean Eng. 31 (11–12), 1407–1421. https://doi.org/10.1016/j.oceaneng.2004.03.004. Aug.

Falcão, A.F.O., Henriques, J.C.C., 2014. Model-prototype similarity of oscillating-water-column wave energy converters. Jun Int. J. Mar. Energy 6, 18–34. https://doi.org/10.1016/j.ijome.2014.05.002.

Falcão, A.F.O., Henriques, J.C.C., 2016. Oscillating-water-column wave energy converters and air turbines: a review. Renew. Energy 85, 1391–1424. https://doi.org/10.1016/j.renene.2015.07.086. Jan.

Falcão, A.F.O., Sarmento, A.J.N.A., Gato, L.M.C., Brito-Melo, A., 2020. The Pico OWC wave power plant: its lifetime from conception to closure 1986–2018. Appl. Ocean Res. 98, 102104 https://doi.org/10.1016/j.apor.2020.102104. May.

Farrell, N., Donoghue, C.O., Morrissey, K., 2015. Quantifying the uncertainty of wave energy conversion device cost for policy appraisal: an Irish case study. Mar Energy Pol. 78, 62–77. https://doi.org/10.1016/j.enpol.2014.11.029.

Garcia-Teruel, A., Forehand, D.I.M., 2021. A review of geometry optimisation of wave energy converters. Renew. Sustain. Energy Rev. 139, 110593 https://doi.org/10.1016/j.rser.2020.110593. Apr.

Gubesch, E., Abdussamie, N., Penesis, I., Chin, C., 2022. Maximising the hydrodynamic performance of offshore oscillating water column wave energy converters. Appl. Energy 308, 118304. https://doi.org/10.1016/j.apenergy.2021.118304. Feb.

Helsel, y D.R., Hirsch, R.M., Ryberg Karen, R., Archfield, S.A., Gilroy, E.J., 2020. Statistical methods in water resources, *Chapter 3 of section A, statistical analysis*, U.S. Department of the interior. Virginia: U.S. Geological Survey James F. Reilly II, Direct. https://doi.org/10.3133/tm4a3 [Online]. Available:

Hersbach, H., et al., 2020. The ERA5 global reanalysis. Q. J. R. Meteorol. Soc. 146 (730), 1999–2049. https://doi.org/10.1002/qj.3803.

Ibarra-Berastegi, G., et al., 2021. The power flow and the wave energy flux at an operational wave farm: findings from Mutriku, Bay of Biscay. Ocean Eng. 227, 108654 https://doi.org/10.1016/j.oceaneng.2021.108654. May.

IPCC, 2013. *Climate Change 2013: The Physical Science Basis. Contribution of Working Group I to the Fifth Assessment Report of the Intergovernmental Panel on Climate Change*. Cambridge University Press, Cambridge, United Kingdom and New York, NY, USA, pp. 1535–pp.

IPCC, 2019. [H.-O. Pörtner, D.C. Roberts, V. Masson-Delmotte, P. Zhai, M. Tignor, E. Poloczanska, K. Mintenbeck, A. Alegría, M. Nicolai, A. Okem, J. Petzold, B. Rama, N. M. Weyer (eds.)]. IPCC Special Report on the Ocean and Cryosphere in a Changing Climate Cambridge University Press, Cambridge, UK and New York, NY, USA, 755 pp. https://doi.org/10.1017/9781009157964, first ed. Cambridge University Press.

Kendall, M.G., 1938. A New Measure of Rank Correlation 30 (1/2), 81–93.

Komen, G.J., Cavaleri, L., Donelan, M., Hasselmann, K., Hasselmann, S., Janssen, P.A.E. M., 1994. Dynamics and Modelling of Ocean wavesKomen, G.J.L. Cavaleri, M. Donelan, K. Hasselmann, S. Hasselmann, and P.A.E.M. Janssen. Cambridge University Press, Cambridge, U.K., p. 532

De Leo, F., Besio, G., Mentaschi, L., 2021a. Trends and variability of ocean waves under RCP8.5 emission scenario in the Mediterranean Sea. Jan Ocean Dynam. 71 (1), 97–117. https://doi.org/10.1007/s10236-020-01419-8.

De Leo, F., Besio, G., Briganti, R., Vanem, E., 2021b. Non-stationary extreme value analysis of sea states based on linear trends. Analysis of annual maxima series of significant wave height and peak period in the Mediterranean Sea. Coast. Eng. 167, 103896 https://doi.org/10.1016/j.coastaleng.2021.103896. Aug.

Liberti, L., Carillo, A., Sannino, G., 2013. Wave energy resource assessment in the Mediterranean, the Italian perspective. Renew. Energy 50, 938–949. https://doi.org/10.1016/j.renene.2012.08.023. Feb.

Lobeto, H., Menendez, M., Losada, I.J., 2021. Future behavior of wind wave extremes due to climate change. Sci. Rep. 11 (1), 7869. https://doi.org/10.1038/s41598-021-86524-4. Dec.

Mackay, E.B.L., Bahaj, A.S., Challenor, P.G., 2010. Uncertainty in wave energy resource assessment. Part 1: Historic data. Renew. Energy 35 (8), 1792–1808. https://doi.org/10.1016/j.renene.2009.10.026. Aug.

Mattiazzo, G., 2019. State of the art and perspectives of wave energy in the Mediterranean Sea: backstage of ISWEC. Front. Energy Res. 7. Mar. 09, 2022. [Online]. Available: https://www.frontiersin.org/article/10.3389/fenrg.2019.00114.

Mentaschi, L., Vousdoukas, M.I., Voukouvalas, E., Dosio, A., Feyen, L., 2017. Global changes of extreme coastal wave energy fluxes triggered by intensified

teleconnection patterns. Geophys. Res. Lett. 44 (5), 2416–2426. https://doi.org/10.1002/2016GL072488. Mar.
Mérigaud, A., Ringwood, J.V., 2018. Power production assessment for wave energy converters: overcoming the perils of the power matrix. Proc. Inst. Mech. Eng. Part M J. Eng. Marit. Environ. 232 (1), 50–70. https://doi.org/10.1177/1475090217731671. Feb.
Morim, J., Hemer, M., Cartwright, N., Strauss, D., Andutta, F., 2018. On the concordance of 21st century wind-wave climate projections. Aug Global Planet. Change 167, 160–171. https://doi.org/10.1016/j.gloplacha.2018.05.005.
Morim, J., et al., 2019. Robustness and uncertainties in global multivariate wind-wave climate projections. Sep Nat. Clim. Change 9 (9), 711–718. https://doi.org/10.1038/s41558-019-0542-5.
O'Grady, J.G., Hemer, M.A., McInnes, K.L., Trenham, C.E., Stephenson, A.G., 2021. Projected incremental changes to extreme wind-driven wave heights for the twenty-first century. Sci. Rep. 11 (1), 8826. https://doi.org/10.1038/s41598-021-87358-w. Apr.
Penalba, M., Giorgi, G., Ringwood, J.V., 2017. Mathematical modelling of wave energy converters: a review of nonlinear approaches. Renew. Sustain. Energy Rev. 78, 1188–1207. C.
Ramos, V., Ringwood, J.V., 2016. Exploring the utility and effectiveness of the IEC (International Electrotechnical Commission) wave energy resource assessment and characterisation standard: a case study. Jul Energy 107, 668–682. https://doi.org/10.1016/j.energy.2016.04.053.
Robertson, B., Bailey, H., Buckham, B., 2019. Resource assessment parameterization impact on wave energy converter power production and mooring loads. Appl. Energy 244, 1–15. https://doi.org/10.1016/j.apenergy.2019.03.208. Jun.
Salvadori, G., Tomasicchio, G.R., D'Alessandro, F., Lusito, L., Francone, A., 2020. Multivariate sea storm hindcasting and design: the isotropic buoy-ungauged generator procedure. Sci. Rep. 10 (1), 20517 https://doi.org/10.1038/s41598-020-77329-y. Dec.
Sen, P.K., 1968. Estimates of the regression coefficient based on Kendall's Tau. J. Am. Stat. Assoc. 63 (324), 1379–1389. https://doi.org/10.1080/01621459.1968.10480934. Dec.
Sharmar, V.D., Markina, M. Yu, Gulev, S.K., 2021. Global ocean wind-wave model hindcasts forced by different reanalyzes: a comparative assessment. J. Geophys. Res. Oceans 126 (1). https://doi.org/10.1029/2020JC016710. Jan.
Sheng, W., Li, H., 2017. A method for energy and resource assessment of waves in finite water depths. Energies 10 (4), 460. https://doi.org/10.3390/en10040460. Apr.
Simonetti, I., Cappietti, L., 2019. In: The Impact of Modelling Air Compressibility in the Selection of Optimal OWC Design Parameters in Site Specific Wave Conditions, 10. Ocean Renewable Energy, Glasgow, Scotland, UK, Jun. https://doi.org/10.1115/OMAE2019-96123. V010T09A041.
Simonetti, I., Cappietti, L., Elsafti, H., Oumeraci, H., 2017. Optimization of the geometry and the turbine induced damping for fixed detached and asymmetric OWC devices: a numerical study. Energy 139, 1197–1209. https://doi.org/10.1016/j.energy.2017.08.033. Nov.
Simonetti, I., Cappietti, L., Oumeraci, H., 2018a. An empirical model as a supporting tool to optimize the main design parameters of a stationary oscillating water column wave energy converter. Appl. Energy 231, 1205–1215. https://doi.org/10.1016/j.apenergy.2018.09.100. Dec.
Simonetti, I., Cappietti, L., Elsafti, H., Oumeraci, H., 2018b. Evaluation of air compressibility effects on the performance of fixed OWC wave energy converters using CFD modelling. Renew. Energy 119, 741–753. https://doi.org/10.1016/j.renene.2017.12.027. Apr.
Têtu, A., Fernandez Chozas, J., 2021. A proposed guidance for the economic assessment of wave energy converters at early development stages. Aug Energies 14 (15), 4699. https://doi.org/10.3390/en14154699.
Ulazia, A., Esnaola, G., Serras, P., Penalba, M., 2020. On the impact of long-term wave trends on the geometry optimisation of oscillating water column wave energy converters. Energy 206, 118146. https://doi.org/10.1016/j.energy.2020.118146. Sep.
Vannucchi, V., Cappietti, L., 2016. Wave energy assessment and performance estimation of state of the art wave energy converters in Italian Hotspots. Sustainability 8 (12), 1300. https://doi.org/10.3390/su8121300. Dec.
Gunther, H.; Lionello, P., Janssen, P. A. E. M., Bertotti, L., Bruning, C., Carretero, J. C., Cavaleri, L., Guillaume, A., B. Hansen, Hasselmann, S., Hasselmann, K., de las Heras, M., Hollingsworth, A., Holt M, Lefevre, J. M. and Portz, R, 1992. *Implementation of a third generation wave ocean model at the European Center for Medium-Range Weather Forecast*, vol. Final report for EC Contract SC1-0013-C(GDF).